catalysts

MDPI

Review

Zirconium Phosphates and Phosphonates: Applications in Catalysis

Anna Donnadio [1], Monica Pica [1], Morena Nocchetti [1] and Oriana Piermatti [2,*]

[1] Dipartimento di Scienze Farmaceutiche, Università degli Studi di Perugia, Via del Liceo 1, 06123 Perugia, Italy; anna.donnadio@unipg.it (A.D.); monica.pica@unipg.it (M.P.); morena.nocchetti@unipg.it (M.N.)
[2] Dipartimento di Chimica, Biologia e Biotecnologie, Università degli Studi di Perugia, Via Elce di Sotto 8, 06123 Perugia, Italy
* Correspondence: oriana.piermatti@unipg.it

Abstract: This review covers recent advancements in the use of zirconium phosphates and phosphonates (ZrPs) as catalysts or catalyst supports for a variety of reactions, including biomass conversion, acid–base catalysis, hydrogenation, oxidation, and C-C coupling reactions, from 2015 to the present. The discussion emphasizes the intrinsic catalytic properties of ZrPs, focusing on how surface acidity, hydrophobic/hydrophilic balance, textural properties, and particle morphology influence their catalytic performance across various reactions. Additionally, this review thoroughly examines the use of ZrPs as supports for catalytic species, ranging from organometallic complexes and metal ions to noble metals and metal oxide nanoparticles. In these applications, ZrPs not only enhance the dispersion and stabilization of active catalytic species but also facilitate their recovery and reuse due to their robust immobilization on the solid support. This dual functionality underscores the importance of ZrPs in promoting efficient, selective, and sustainable catalytic processes, making them essential to the advancement of green chemistry.

Keywords: zirconium phosphates; zirconium phosphonates; heterogeneous catalysis

check for updates

Citation: Donnadio, A.; Pica, M.; Nocchetti, M.; Piermatti, O. Zirconium Phosphates and Phosphonates: Applications in Catalysis. *Catalysts* **2024**, *14*, 733. https://doi.org/10.3390/catal14100733

Academic Editor: Xiujie Li

Received: 13 September 2024
Revised: 9 October 2024
Accepted: 17 October 2024
Published: 19 October 2024

Copyright: © 2024 by the authors. Licensee MDPI, Basel, Switzerland. This article is an open access article distributed under the terms and conditions of the Creative Commons Attribution (CC BY) license (https://creativecommons.org/licenses/by/4.0/).

1. Introduction

Catalysis plays a pivotal role in industrial production, scientific research, and even in everyday life, underlining its importance. The request for optimal catalytic activity and selectivity has driven extensive efforts in catalyst design, with particular emphasis on catalyst recovery and reuse. While classical homogeneous catalytic systems have proven notable efficiency, their separation from reaction mixtures poses challenges, necessitating costly and laborious purification procedures. Moreover, the intrinsic costliness of noble metal and/or ligand components limits the application of homogeneous catalysts in industrial applications. Heterogeneous catalyst systems offer advantages such as simplified recovery, provided that catalyst activity is maintained during reuse cycles, as well as the ability to control selectivity and improve efficiency [1–3].

Faced with growing ecological and economic needs, catalysis takes on a fundamental role in green chemistry and the sustainable environment and energy [4,5]. The benefits of heterogeneous catalysis, including optimized product isolation, efficient catalyst recycling, reduced metal traces in products, and enhanced process control, significantly reduce the costs associated with chemical transformations. The advantages offered by heterogeneous catalysis have stimulated the exploration of alternative solid catalysts and the development of new supports for the heterogenization of conventional homogeneous systems. These systems are in tune with both the chemical and sustainability perspectives, aligning with modern synthesis methodologies that prioritize efficiency and environmental responsibility [6–9].

Layered zirconium phosphates and phosphonates (ZrPs) have emerged as intriguing and versatile materials in the realm of catalysis, captivating the attention of researchers due

to their unique structural characteristics and inherent physical and chemical properties. They show excellent chemical and thermal stability both in their amorphous and crystalline phases, a superior ion exchange capacity, a high surface area due to their layered and porous structures, and good biocompatibility. The layered structure of ZrPs provides a platform onto which organic groups with diverse functionalities can be intricately attached (e.g., acid, basic, polar, hydrophobic, chiral, or chelating groups) or can be lodged (metal nanoparticles). This feature, together with a feasible preparation by a self-assembly approach, allows for the fine-tuning of the material surface properties through a judicious choice of the building blocks, enabling the customization of active sites for specific catalytic reactions. The ability to tailor these materials at the nanoscale presents an exciting avenue for the development of catalysts with enhanced efficiency and selectivity [10–18].

This review aims to explore the catalytic potential of layered zirconium phosphates and phosphonates by examining their preparation methods, structural features, and the catalytic applications they exhibit. As we navigate through their unique properties and recent advancements in the field, it becomes evident that these materials hold promise as catalysts or catalyst supports in various environmentally benign synthetic strategies. The subsequent sections will explore the specific roles of zirconium phosphates and phosphonates in catalysis, shedding light on their contributions to the advancement of sustainable and efficient chemical processes.

2. Zirconium Phosphates and Phosphonates (ZrPs): Structural Features and Synthetic Approaches

Since 1964, when Clearfield obtained crystalline α-zirconium monohydrogen phosphate (α-$Zr(HPO_4)_2 \cdot H_2O$, α-ZrP), many studies have focused on layered zirconium phosphates and phosphonates, especially on the development of an innovative synthetic approach and, consequently, on the implementation of the different fields of application.

Layered zirconium phosphates exhibit two main types of structures, the alpha and gamma types (Figure 1). In α-zirconium phosphate ($Zr(O_3POH)_2 \cdot H_2O$), each layer consists of a single plane of Zr atoms bonded by tri-dentate monohydrogen phosphate groups. These groups are located alternately above and below the plane. Each Zr atom is coordinated in an octahedral shape by the oxygen atoms of six phosphate groups, and each phosphate group shares oxygen atoms with three Zr atoms (Figure 1a). In γ-zirconium phosphate ($Zr(PO_4)(O_2P(OH)_2) \cdot 2H_2O$, γ-ZrP), the layer is made of two parallel planes of Zr atoms bridged by tetracoordinated inner PO_4^{3-} (Figure 1b) groups. The external di-hydrogen phosphate groups ($(O_2P(OH)_2)^-$) face both layer sides, and each of them is bonded to two Zr atoms through unprotonated oxygen atoms. In both cases, the crystallization water molecules are located in the interlayer region.

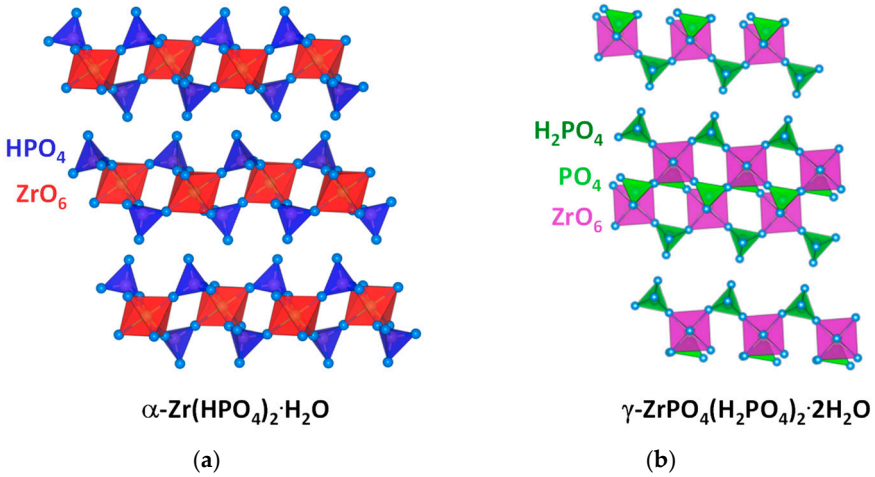


Figure 1. Schematic view of (**a**) α-ZrP and (**b**) γ-ZrP structures.

Organic derivatives with both α- and γ- structures can also be prepared. In addition to the more well-known α- and γ-structures, depending on the synthetic methods and the molecular structure of the phosphonic acids, a large variety of structural archetypes with different dimensionality has been found [19].

The increasing interest in zirconium phosphate and phosphonates (ZrPs) is mainly attributed to their superior properties including thermal stability, ion exchange and intercalation capability, and proton conductivity. The tunability of textural properties, such as crystallinity degree, specific surface area, and acid–base properties, can be controlled simply by modifying the synthetic conditions or the composition of the layers. Indeed, ZrPs can be easily prepared using a self-assembly approach, and the desired chemical and physical properties can be finely tuned by a clever choice of the building blocks.

Crystalline ZrPs with micrometric or nanometric dimensions can be directly synthesized by hydrothermal, refluxing, sol–gel, microemulsion, and microwave methods (Figure 2). The effect of the preparation method on the textural properties of materials has recently been reviewed [17,20–23]. Briefly, these synthetic procedures foresee the reaction of the building blocks, inorganic or organic zirconium (IV) salts with phosphoric acid, phosphonic acids, or a mixture of phosphoric/phosphonic acids, assisted, if needed, by hydrofluoric acid, oxalic acid, and formamide as complexing agents. Different morphologies, sizes, and crystallinity degrees can be obtained through the fine control of the reaction conditions such as temperature, time, reagents, solvents, and ratios [24]. Zirconium phosphonates can also be prepared starting from alpha or gamma zirconium phosphate by the topotactic exchange of phosphate by phosphonate groups. This procedure allows for a wide variety of organic pendants to be anchored without modifying the layer structure [21,25]. For α-structures, the topotactic exchange reaction is effective only when using nanocrystalline α-ZrP as a starting material: this approach is preferred when direct synthesis is hindered by the different solubility levels of the various building blocks. Nanocrystalline α-type zirconium phosphate and phosphonates exhibit several advantages with respect to the corresponding microcrystalline compounds, among them being faster and milder synthetic conditions and higher reactivity.

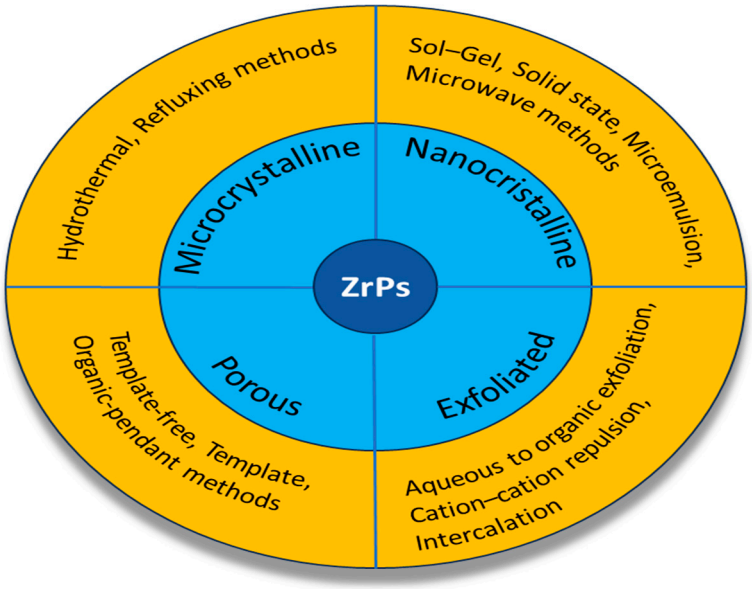


Figure 2. Schematic illustration of typical methods for synthesizing ZrPs with different textural properties.

To meet the growing demand for environmentally friendly approaches, several efforts are focused on developing solid-state methods that minimize the excessive use of acids and harmful solvents. α-ZrP can be obtained by mixing concentrated phosphoric acid and $ZrOCl_2 \cdot 8H_2O$, using low P/Zr molar ratios, and heating at a temperature ranging from 25 to 120 °C for 24 h [26]. Intercalated zirconium phosphates with alkali metals have been prepared by grinding $ZrOCl_2 \cdot 8H_2O$ with Na_2HPO_4 or $(NH_4)_2HPO_4$ and heating at 120 °C for 24 h [27,28]. A similar procedure was followed to prepare $K_2Zr(PO_4)_2$, where ZrO_2 and KPO_3 were mixed and then heated at 750 °C for 24 h [29].

Mesoporous ZrPs with a high surface area and tailored pore size are obtained by templating routs using cationic [30], anionic [31], or neutral [32] surfactants or by sol–gel synthesis in the presence of specific polymers [33]. Other strategies involve template-free synthesis and the preparation of ZrPs by linking pendant organic groups (Figure 2) [15–17,34–36]. The latter strategy consists of linking adjacent layers by using a low amount of diphosphonate groups, such as 1,4-benzenediphosphonate, diluted with small monophosphonate or phosphite groups.

To increase accessibility to catalyst surfaces, layered ZrPs can be exfoliated in individual sheets or a few packed lamellae, forming a colloidal dispersion. The most used strategy to obtain colloidal dispersions is the "top-down" approach, consisting of post-synthesis treatments of ZrPs, including an aqueous to organic exfoliation system, cation–cation repulsion, and intercalation leading to exfoliation (Figure 2) [37].

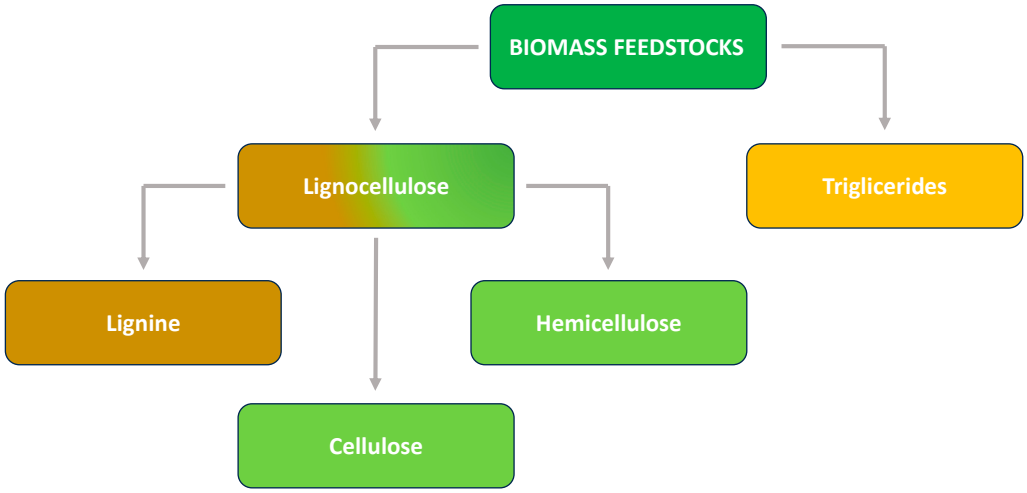
The ion exchange properties of ZrPs, containing exchangeable protons, have also been exploited to prepare materials containing metal ions or metal complexes. In general, these catalysts have been prepared by exchanging the acidic protons for catalytically active cations. The exchanged compounds could also be treated with reducing agents, thus obtaining metallic nanoparticles [11,23].

3. ZrPs as Solid Acid Catalysts

Zirconium phosphate and its organic derivatives, zirconium phosphonates, have been recognized as promising solid acid catalysts due to their unique properties such as tunable acidity and basicity, excellent thermal and chemical stability, high water tolerance, and low cost. The presence of P-OH groups on the surface of layers is responsible for Brønsted acid properties, while Zr^{4+} centers provide Lewis acid properties. The preparation method significantly affects the surface characteristics and acid–base properties [16]. A high surface area is essential to increase exposed acid sites and facilitate interaction with substrates. Moreover, the hydrophobicity of the solid acid surface affects catalytic activity, which can be modulated by introducing different hydrophobic R groups on the layers. Indeed, the presence of hydrophobic R groups on the surface of zirconium phosphate/phosphonates can not only impact the surface properties, such as the specific surface area and micro- and meso-porosity, but also facilitate the diffusion of reagents towards acidic sites, thereby increasing catalytic activity [35,36].

A wide range of acid-catalyzed reactions using ZrPs as heterogeneous catalysts are reported in the literature (Tables 1 and 2).

The valorization process for biomass conversion has been the subject of intense research efforts in recent years. Lignocellulosic biomass, mainly composed of lignin, cellulose, and hemicellulose, represents the most accessible renewable carbon resource, and it is used for the production of fuels, high-value-added chemicals, and new bio-based materials such as bioplastics (Scheme 1). Biomass conversion can be achieved through various reactions, including hydrogenation, dehydrogenation, deoxygenation/hydrogenolysis, and oxidation, often combined with acid-/base-catalyzed reactions like hydrolysis and dehydration to realize one-pot multistep processes.



Scheme 1. Biomass feedstock composition.

Among the various solid catalysts developed for biomass and derivative conversion, zirconium phosphates (ZrPs) stand out for their high thermal stability and water tolerance as well as the presence of tunable acidic sites. These characteristics are particularly advantageous for biomass conversions that occur at high temperatures and in aqueous media. The synergy between metal centers and acidic sites in modified ZrPs catalysts makes them suitable for a wide range of specific chemical transformations, making them promising for the sustainable valorization of biomass [12] (Table 1).

Table 1. The use of zirconium phosphates as heterogeneous catalysts for acid-catalyzed biomass valorization processes.

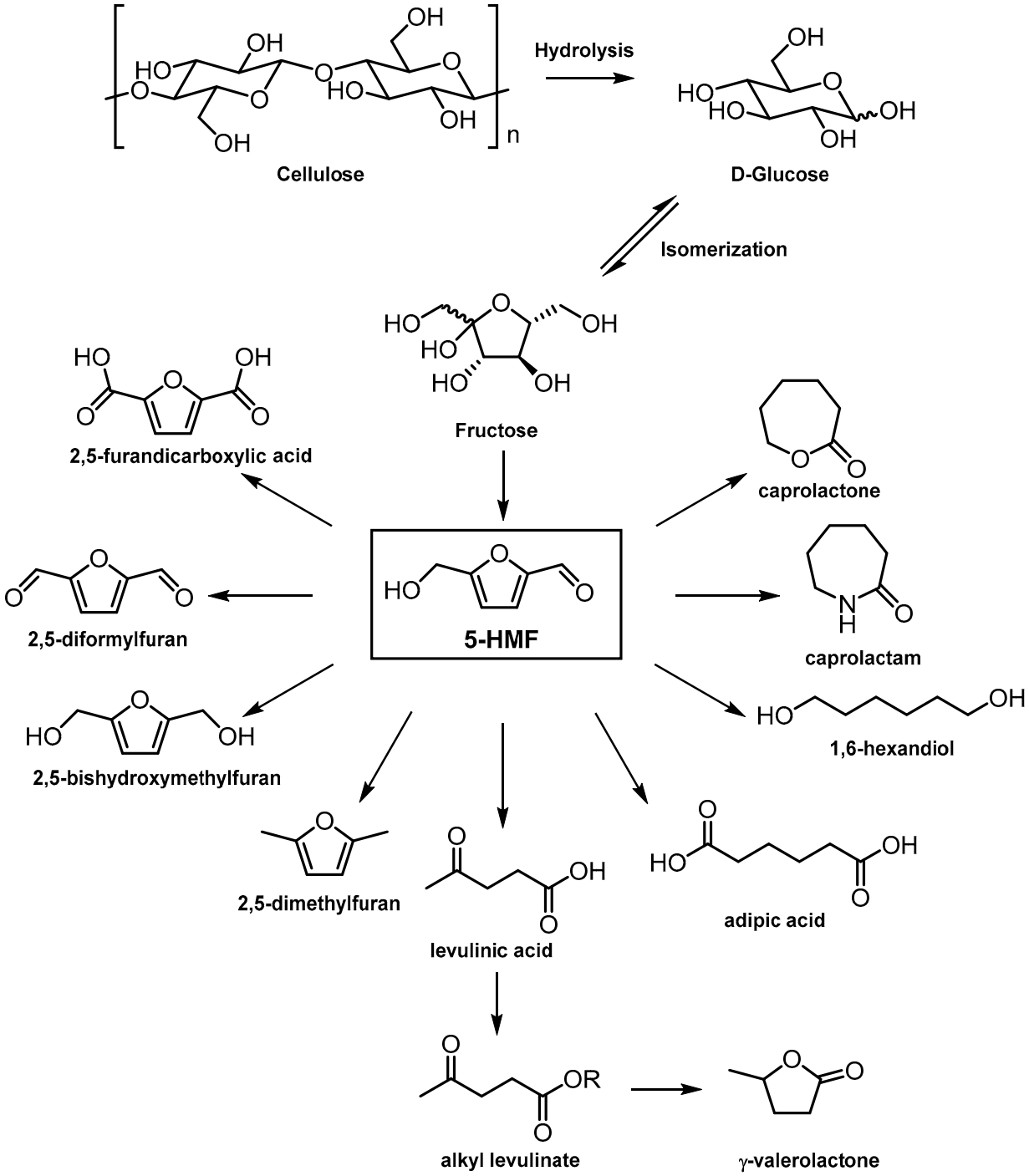
Catalyst	Preparation Methods	BET Surface Area m^2/g	Catalyzation Process	Ref.
ZrP mesoporous	Hydrothermal method (CTAB as template), calcination at 550 °C	407	Dehydration of sugar to 5-HMF	[38]
ZrP-x mesoporous P/Zr = 0.25–1.25	Evaporation-induced self-assembly (F-127 as template), calcination at 500 °C	118.5–163.8		[39]
ZrP amorphous	Precipitation, calcination at 400 °C	108		[40]
ZrP mesoporous	Hydrothermal method (P-123 as template), calcination temp. 500–800 °C	213–114.5		[41]
ZrP-x amorphous P/Zr = 0.5–2	Precipitation, calcination at 400 °C	104.6–160.5		[42]
ZrP-S amorphous	Acid-modified ZrP with oleum SO_3	73.6		[43]
ZrP-S amorphous	Acid-modified ZrP with oleum SO_3	73.6	Dehydration of sorbitol to isosorbide	[43]
ZrP porous	Hydrothermal method (Pluronic P123 as template), calcination at 450 °C	148		[44]
ZrP porous	Sol–gel	600	Dehydration of xylose to furfural	[45]
ZrP amorphous	Hydrothermal method (P-123 as template), calcination at 400 °C	232	Hydrogenation of furfural to FA	[46]
ZrP-S	Acid-modified ZrP with H_2SO_4 S/Zr = 0–0.19	14–67	Hydrogenation of FA to ethyl levulinate	[47]
ZrP-SAPO-34 P/Zr = 0.5–2	Precipitation in presence of SAPO-34 zeolite powder, calcination at 400 °C	424–290	Hydrogenation of FA to GVL	[48]
ZrP_HT, ZrP_CT	Hydrothermal or coprecipitation method, calcination at 550 °C	195.0, 192.6		[49]

Table 1. *Cont.*

Catalyst	Preparation Methods	BET Surface Area m^2/g	Catalyzation Process	Ref.
ZrP-x amorphous P/Zr = 0.5–2	Precipitation and calcination at 400 °C	143.5–279.6	Hydrogenation of alkyl levulinate to GVL	[50]
ZrP-$PrSO_3H$	ZrP modified with propylsulfonic acid groups via post-grafting	142.7	Hydrogenation of xylose to alkyl levulinate	[51]
ZrP-x mesoporous P/Zr = 1.5–2.5	Hydrothermal method (CTAB as template), calcination at 550 °C	366.1–262	Esterification of levulinic acid	[52]
α-ZrP and γ-ZrP	Precipitation and reflux	-		[53]
ZrPx-KIT, ZrPx-SBA P/Zr= 0–2	ZrP grafted mesoporous silicas	583.0–446.6	p-Xylene production from biomass-derived 2,5-dimethylfuran	[54]
ZrPx P/Zr = 1–3	Hydrothermal method, calcination at 550 °C	196.5–410.9		[55]
SO_3H-ZrP single layer nanosheets	Surface modification of exfoliated α-ZrP with propylsulfonic acid groups via post-grafting	-	Biodiesel production	[56]
ZP-P[SIH]-x composite, x = 1, 2, 3	Hybridization of poly(ionic liquid) (P[SIH]) with mesoporous zirconium phenylvinyl phosphonate	180–103		[57]
ZrP amorphous	Precipitation, calcination at 400 °C	101.3	Dehydration of glycerol to acrolein	[58]
ZrP-x porous P/Zr = 0.33–3	Sol–gel	442.3–107.0		[59]
$Zr_x(PO_4)_y(SO_4)_z$	Co-precipitation	11–15	Acetylation glycerol	[60]
PSA/K-ZrP-x x = 0.2–3	p-Phenolsulfonic acid grafted onto the surface of KH560-modified α-ZrP	6.3–1.7		[61]
ZrP	Hydrothermal method, calcination at temp. of 200–600 °C	43.6–47.0	Acetalization of glycerol (solketal)	[62]
ZrPPx flower-like x = 0–100% phenyl phosphonic acid	Hydrothermal method, calcination at 200 °C	43.6–8.1		[63]
ZPS-PVPA-SO_3H	Sulfonic acid-functionalized zirconium poly(styrene-phenylvinyl-phosphonate)-phosphate	-	Epoxidation of soybean oil	[64]

5-Hydroxymethyl-2-furfural (5-HMF) is a key chemical intermediate derived from biomass, recognized for its versatility in producing a wide range of bio-based products. HMF serves as a valuable precursor for polymers (e.g., 2,5-diformylfuran and 2,5-furandicarboxylic acid), fuels (e.g., 2,5-dimethylfuran), and solvents (levulinic acid). Its multifunctional structure, featuring both aldehyde and hydroxyl groups, allows for the creation of various high-value chemicals, pharmaceuticals, and materials through reactions like hydrogenation, oxidation, rehydration, and polymerization (Scheme 2) [65]. It is synthesized from the dehydration of sugars such as fructose, glucose, and cellulose. Typically, both Lewis and Brønsted acid catalysts are involved in converting sugar into fructose and then into 5-HMF. Recent advancements in heterogeneous catalytic systems have improved 5-HMF production efficiency, making it a crucial component in the development of green chemistry and sustainable biomass utilization. Among mesostructured solid acid catalysts, zirconium phosphates, with their high surface area and balanced Lewis and Brønsted acid sites, are particularly attractive. Some recent examples are briefly described below.

In 2015, a mesoporous ZrP with a high surface area (407 m^2/g) was obtained via the hydrothermal method in the presence of cetyltrimethylammonium bromide (CTAB) as a template and calcination at 550 °C by Mugweru and coworkers [38]. The mesoporous zirconium phosphate exhibited excellent catalytic activity in a 3:1 ratio of water/diglyme as the reaction medium, saturated with NaCl at 150 °C. Fructose, glucose, and sucrose provide 5-HMF in 80%, 63%, and 53%, respectively. The catalyst, after being recycled five times, showed a negligible reduction in activity.



Scheme 2. Target molecules from 5-hydroxymethyl-2-furfural (5-HMF).

In the same year, Chou and coworkers obtained mesoporous ZrPs with different P/Zr ratios through the self-assembly strategy (F-127 template) and calcination at 500 °C [39]. The best catalytic activity was obtained for P/Zr = 0.75, which showed excellent catalytic activity and good reusability in fructose dehydration to 5-HMF in DMSO at 120 °C. The mesoporous structure was retained even after twelve cycles, likely due to the ordered mesoporous structure and high thermal stability.

The microwave-assisted dehydration of fructose and inulin to 5-HMF in water, catalyzed by amorphous ZrP obtained through precipitation and calcination at 140 °C, was reported in 2017 by Raspolli Galletti and coworkers [40]. The catalytic activity of ZrP was compared to that of niobium phosphate, and the performance was related to their different acid characteristics. ZrP was reused three times with only a slight decrease in conversion and selectivity. The IR spectrum of the recovered ZrP showed organic deposits on the catalyst surface that can be reactivated by acetone washing.

In 2018, mesoporous ZrPs with a large pore diameter (>9 nm) were prepared hydrothermally in water using P123 as a template by Wook Bae and coworkers [41]. They investigated the effects of the calcination temperature (500−800 °C) on the textural and acidic/basic properties of the mesoporous ZrP and its catalytic performance for glucose dehydration to 5-HMF in pure water as a green reaction medium. Mesoporous ZrP-600, with an appropriate number and strength of Lewis and Brønsted acid and basic sites, efficiently promoted the isomerization of glucose to fructose and its successive dehydration to 5-HMF. The strong Lewis acid and basic sites facilitated glucose isomerization to fructose, which dehydrated exclusively on the weak Brønsted acid sites, resulting in a maximum glucose conversion (83.8%) and 5-HMF yield (46.6%). Additionally, the large pores facilitated diffusion, and the turnover frequency (11.68/h) for glucose to HMF conversion was higher than that of small-pore mesoporous ZrP.

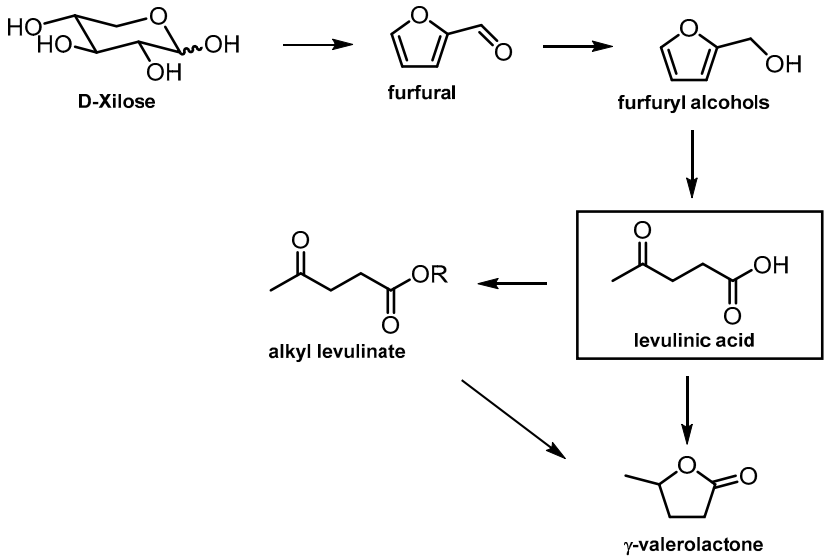
In the same year, Ma and coworkers prepared amorphous ZrPs with different P/Zr ratios through precipitation and calcination at 400 °C for C6-sugar dehydration to 5-HMF [42]. The highest continuous HMF production was observed using fructose over ZrP with P/Zr = 2, which showed the highest surface area, pore volume, and total acidity density. No deactivation was observed after 30 h of time on stream.

In 2019, an amorphous acid-modified ZrP-S was obtained by Hou and coworkers by treating ZrP with 20% oleum, and its activity was compared with both amorphous and crystalline ZrP [43]. The acid treatment enhanced the amounts and the strength of Brønsted and Lewis acidic sites, while the molar ratio of Brønsted to Lewis acid sites remained unchanged. Additionally, acid modification induced the exfoliation of the amorphous structure, resulting in the formation of very thin nanosheets, thereby exposing more active sites for catalytic reactions. The acid-modified ZrP-S catalyst exhibited the highest selectivity (73.4%) for 5-HMF production through the dehydration of fructose, with respect to the non-modified ZrP. It was recycled for up to five times without significant loss of activity, demonstrating chemical and thermal stability as well as high leaching resistance of its acidic sites through consecutive catalytic cycles. Additionally, the same catalyst was also used in the dehydration of sorbitol to isosorbide, an important building block for the production of new polymers and functional materials, showing the highest reactivity and selectivity (73.6%) compared to the non-modified ZrP [43].

The dehydration of sorbitol to isosorbide was also obtained by Cai and coworkers in 2016 by using a porous ZrP prepared by the hydrothermal method with Pluronic P-123 as a template [44]. The catalyst showed complete conversion and high selectivity (73%) to isosorbide production for five consecutive runs, and only a slight decrease in catalytic activity was observed at the sixth run. The promising catalytic performance was attributed to its high surface area and porous structure, which exposed a great quantity of adequate Brønsted acid sites.

Xylose represents an important feedstock from hemicellulose for the preparation of important target molecules, such as furfural, from which levulinic acid and its derivatives can be obtained (Scheme 3).

In 2016, Nakanishi and coworkers reported the preparation of hierarchically porous monolithic ZrP via the sol–gel method [45]. This catalyst featured a high surface area (600 m^2/g) and both micro- and meso-porosity. It was used as a solid acid catalyst for the dehydration of xylose into furfural. The high accessibility of the acidic sites and easy separation of the monolith from the liquid medium resulted in the catalyst having good catalytic activity and recyclability.



Scheme 3. Valorization process for biomass-derived D-xylose.

The transformation of furfural into furfuryl alcohol with a high yield (95.2%) and selectivity (76%) was achieved in 2020 by Srivastava and coworkers via eco-friendly, isopropanol-mediated hydrogenation at 120 °C using amorphous ZrP as a solid catalyst [46]. This catalyst was obtained via hydrothermal synthesis in the presence of P123 as a mesopore-directing agent and calcination at 400 °C. The high activity of ZrP is attributed to its bifunctional nature, possessing both Lewis and Brønsted acidic sites, and the efficient adsorption capacity of furfural. The catalyst exhibits no significant change in activity even after being recycled five times, and the heterogeneity of the catalytic process was demonstrated by a hot filtration test.

In 2019, Wang and coworkers reported the use of modified ZrP with sulfuric acid for the direct production of ethyl levulinate from furfuryl alcohol in ethanol at 200 °C [47]. This modification enhances both the Lewis and Brønsted acidity of zirconium phosphate by adjusting the S/Zr ratio rather than the P/Zr ratio. Higher catalytic activity was observed (100% conversion; 97.8% selectivity) in comparison to unmodified ZrP. The catalyst was reused for three runs with a slight decrease in catalytic activity due to organic deposits on the surface, but with calcination in air at 550 °C, a recovery of catalytic activity was observed in the fourth run.

The one-pot synthesis of γ-valerolactone (GVL) from furfural was achieved in 2021 by Lin and coworkers by using isopropanol as an H-donor and solvent and SAPO-34 zeolite-supported ZrP as solid acid catalysts [48]. The acidic properties of the catalyst were modulated by adjusting the P/Zr ratio, with the best results obtained for P/Zr = 1. This ratio provided relatively strong Lewis acid sites and an appropriate Lewis/Brønsted site ratio, resulting in full furfural conversion and GVL selectivity of up to 80.0%. The recycling tests showed constant full conversion, but the selectivity of GVL gradually decreased, probably due to carbon deposits on the solid catalyst surface that reduced both the number of acidic sites and the BET surface area. After removing the carbon deposits by calcining the spent catalyst at 400 °C, a recovery of both textural properties and catalytic activity was observed.

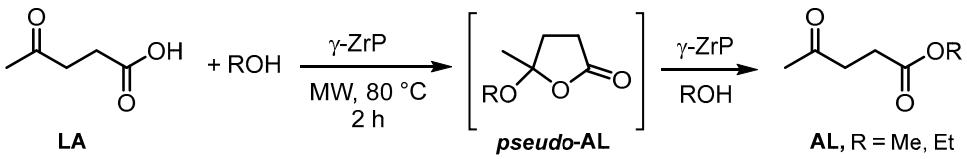
The same process was investigated in 2022 by He and coworkers [49]. The authors used ZrP obtained via the hydrothermal (ZrP-HT) or coprecipitation method (ZrP-CT) as a solid acid catalyst. ZrP-HT calcined at 550 °C, with a larger density of acidic sites, showed superior catalytic activity (42.7% yield of GVL) compared to ZrP-CT. The used catalyst needed regeneration by calcination to recover its activity. The slight deactivation over reuse was attributed to the reduction in the acidic site density due to mesopore collapse.

The catalytic transfer hydrogenation of butyl levulinate to GVL over ZrP with adjustable Lewis and Brønsted acid sites, using isopropanol as the hydrogen donor, was achieved in 2017 by Li and coworkers [50]. The hydrophobicity, strength of Lewis acid sites, and Lewis/Brønsted acidic site ratio were tuned through P/Zr adjustment, resulting in excellent catalytic activity (for P/Zr = 1, 98.1% conversion and 95.7% yield of GVL). The catalyst maintained relatively satisfactory activity for 10 runs. The loss of activity was attributed to an increase in the carbon content on the surface of the solid catalyst along with reductions in the surface area and pore volume. The spent catalyst after 10 runs was effectively regenerated by calcination (97.2% conversion; 94.8% yield of GVL).

In 2022, Saraji and coworkers prepared a modified ZrP with propyl sulfonic acid groups via a post-grafting method, aimed at the production of alkyl levulinate from xylose [51]. The maximum n-butyl levulinate yield was 82% at 170 °C after 6 h, while the maximum ethyl levulinate yield was 49% at 150 °C after 6 h. Alcohol plays a crucial role in xylose dehydration: n-butanol, due to its higher lipophilicity and boiling point, exhibited better levulinate yields. However, n-butanol and ethanol display a similar ability as H-donors. The catalyst showed stable catalytic activity up to the fourth run, after which the alkyl levulinate yield decreased due to the leaching of propyl sulfonic acid groups.

Mesoporous ZrPs with a high surface area and different P/Zr ratios were obtained via the hydrothermal method in the presence of CTAB as a template, followed by calcination at 550 °C, by Chermahini and coworkers in 2021 [52]. The solid catalysts with a P/Zr ratio of 2 showed the highest total acidity and a high surface area, providing the best result for the production of n-butyl levulinate from levulinic acid (80% yield at 120 °C after 8 h).

In 2024, Rocha and Lopes reported the use of layered α-ZrP and γ-ZrP in the esterification of levulinic acid (LA) with ethanol or methanol using either the conventional reflux method or microwave (MW) irradiation [53]. The best conversion and selectivity were achieved with γ-ZrP under MW irradiation at 80 °C for 2 h. The superior catalytic activity of γ-ZrP was attributed to its larger interlayer distance and a higher number of acidic -OH sites within the interlayers and on the surface compared to α-ZrP. These textural properties facilitate the protonation of LA and the subsequent addition of alcohol to the protonated LA, forming a *pseudo*-AL intermediate. The protonation of *pseudo*-AL, followed by a reaction with alcohol, results in the formation of alkyl levulinate (AL) (Scheme 4).



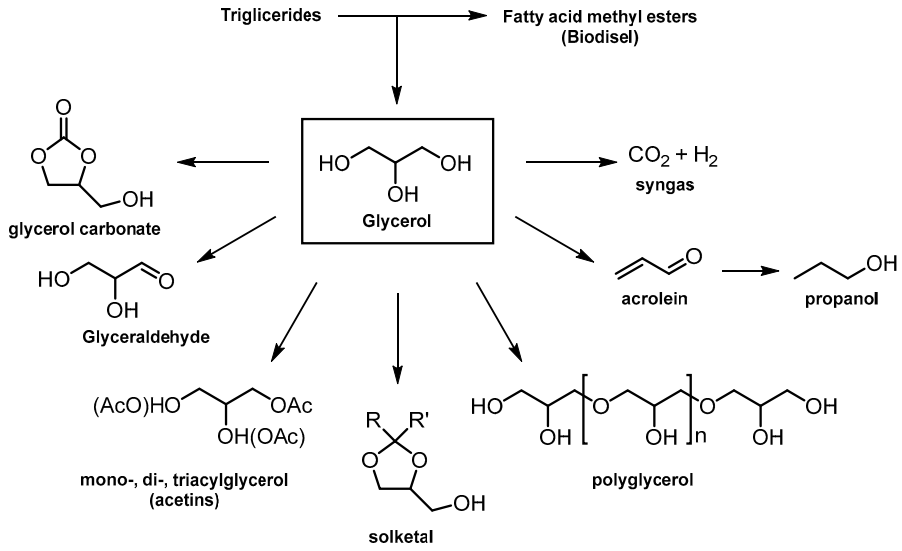
Scheme 4. Levulinic acid (LA) esterification over γ-ZrP under MW irradiation.

The catalytic conversion of biomass-derived furans into renewable aromatic chemicals, such as benzene, toluene, and xylenes, is an important challenge.

In 2020, Dong and coworkers [54] prepared ZrPs with variable P/Zr ratios, grafted on ordered mesoporous silicas with a high surface area (KIT-6, SBA-15, and SiO_2) for the selective production of *p*-xylene by the catalytic reaction of 2,5-dimethylfuran with gaseous ethylene through tandem Diels–Alder cycloaddition and dehydration. The solid acid catalyst $ZrP_{1.5}$-SBA, with a high dispersion of acidic sites and a larger surface area, showed the best catalytic activity (91% conversion with 96% selectivity). Moreover, its catalytic activity and mesopore structure were retained for four runs.

Very recently, the same process was studied by Dong and coworkers using a series of zirconium phosphates (ZrP-x) with various P/Zr ratios obtained through a hydrothermal method [55]. For P/Zr 2.5, they observed a higher surface area (410.9 m^2/g), abundant mesopores, more acidic sites, and a balance between Brønsted and Lewis acidity, which produced high conversion (99.1%) and productivity (72.3 mmol/g·h). The recovered catalyst, regenerated by calcination in air at 500 °C for 4 h to remove the adsorbed carbonaceous species, exhibited stable catalytic activity for up to six runs.

Biodiesel, produced by the transesterification of vegetable and animal fats/oils, is considered an attractive alternative to fossil fuel energy resources. However, large quantities of glycerol are generated as a by-product, necessitating effective approaches for its valorization. Due to its polyfunctional structure with three hydroxyl groups, glycerol can be converted into numerous high-value-added chemicals (Scheme 5).



Scheme 5. Valorization process for fats and oils.

In 2018, Sun and coworkers prepared surface-modified single-layer ZrP nanosheets with propylsulfonic acid (SO_3H@ZrP) using the post-grafting method for the esterification of oleic acid with methanol to produce biodiesel [56]. The catalytic activity of the solid acid was slightly lower than that of liquid H_2SO_4; however, it exhibited higher catalytic activity than the commercial Amberlyst®15. The catalyst was easily recovered and reused for seven runs with only a slight decrease in catalytic activity.

Mesoporous composite materials (ZP-P[SIH]-x) were obtained by Yang and coworkers in 2022 by hybridizing sulfonic acid-functionalized poly(ionic liquid) (P[SIH]) with zirconium phenylvinyl phosphonate (ZP) [57]. The ZP-P[SIH]-2 catalyst showed a high pore volume, excellent hydrophobicity and wettability for the substrates, along with uniformly dispersed acid and base sites for the direct transformation of crude *Euphorbia lathyris L.* oil into biodiesel (93% biodiesel yield). No reduction in catalytic activity was observed until the fourth run.

In 2016, Hou and coworkers [58] achieved the catalytic transformation of glycerol to 1-propanol using sequential two-layer catalysts in a continuous-flow reactor. Amorphous ZrP was packed in the first layer for the dehydration of glycerol into acrolein, and a supported Ru catalyst (2% Ru/SiO_2) was used in the second layer for the sequential hydrogenation of acrolein to 1-propanol. This catalytic system provided complete conversion and 77% selectivity for 1-propanol, along with long-term stability (80 h). Carbonaceous deposits on ZrP were the main reason for deactivation observed after 100 h; however, calcination in air at 500 °C for 4 h regenerated the spent catalyst, which could then be reused for another 100 h with only a slight decrease in selectivity.

In 2018, Chary and coworkers prepared porous ZrPs catalysts with variable P/Zr ratios and a high surface area via the sol–gel method for gas-phase glycerol dehydration to acrolein [59]. The best result was obtained with a P/Zr ratio of 2, achieving 100% conversion and 56% selectivity for acrolein. This superior performance is attributed to the highest total amount of acidic sites and the presence of both weak and moderate acidic regions.

In 2019, mixed zirconium phosphate–sulfate acid catalysts were investigated by Liotta and coworkers for the acetylation of glycerol with acetic acid to obtain acetins as fuel additives [60]. Due to its high acidity, the most selective catalyst was $Zr_4(PO_4)_2(SO_4)_5$,

which was used for recycling experiments for up to five cycles. Despite a modest loss of activity, a significant decrease in selectivity to tri- and diacetin was observed after the first cycle due to the leaching of sulfate groups.

In 2021, Hou and coworkers [61] prepared an organic–inorganic combined solid acid by grafting p-phenolsulfonic acid (PSA) onto the surface of modified zirconium phosphate (K-ZrP). An appropriate molar ratio of PSA and K-ZrP (PSA/K-ZrP-2) increased the acidity as well as the accessibility to acidic sites, showing high performance (81.3% conversion with 97.9% selectivity for mono- and diacetin) and stability for up to five runs in the transesterification between glycerol and methyl acetate.

The same authors in 2019 [62] and 2020 [63] reported the use of layered crystalline ZrP and flower-like zirconium phosphate phenylphosphonate (ZrPP), obtained by the hydrothermal method, in the acetalization of glycerol with acetone to obtain high-value-added solketal. The performance of the catalysts depended mainly on the surface density of the acid sites. For ZrPP, the synergistic effect of acidity and the hydrophilia/hydrophobicity balance could retard deactivation from adsorbed condensation water, allowing for better catalytic performance (90.2% vs. 85.7% conversion) and stability over five runs.

Epoxidized vegetable oils have attracted much attention because they are widely used as plasticizers and stabilizers for polyvinyl chloride (PVC). The epoxidation of soybean oil, typically achieved with peroxyacid, was conducted by Zhao and coworkers in 2019 using sulfonic acid-functionalized zirconium poly(styrene-phenylvinyl-phosphonate)-phosphate (ZPS–PVPA–SO_3H) and tert-butyl hydroperoxide (TBHP) as an oxidant [64]. Recycling tests showed no significant decrease in catalytic activity for five runs, but a drop was observed thereafter. Interestingly, if the catalyst was kept in 2 M of HCl overnight, the catalytic activity was restored for up to the tenth cycle.

Zirconium phosphates and phosphonates have been widely used not only for biomass transformation but also for a large number of acid-catalyzed transformations (Table 2).

Table 2. The use of zirconium phosphates as heterogeneous catalysts for acid-catalyzed transformation.

Catalyst	Preparation Methods	BET Surface Area m^2/g	Catalyzed Process	Ref.
ZrHEDP, ZrATMP, ZrEDTMPS porous	Hydrothermal (CTAB as template)	310–749	Hydrolysis/esterification	[66]
ZrHEDP, ZrATMP, ZrEDTMPS porous	Hydrothermal (CTAB as template)	310–749	CO_2 fixation	[67]
$Zr(H_4L)$ framework	Reflux (HF), H_8L = tetraphenylsilane tetrakis-4-phosphonic acid	-		[68]
CrZrP, $CrZr_2P$ porous	Sol–gel	127.9, 149.3	Oxidation alkanes and alkenes	[69]
ZrP/MCM-41 3–10% ZrP loading	Precipitation in presence of MCM-41, calcination at 400 °C	671–642	Oxidative desulfurization of benzothiophene	[70]
ZrP nanoparticles	Combustion method (550 °C)	Particle size 66 nm	Synthesis of nitriles	[71]
ZrP nanoparticles	Combustion method (550 °C)	Particle size 66 nm	Photocatalytic degradation of dyes	[71]
α-ZrP nanoparticles	Minimal solvent synthesis in polypropylene	Particle size 30 nm		[72]
ZrP amorphous	Reflux and calcination at 600 °C	23.11	Isomerization α-pinene oxide to trans-carveol	[73]
ZrP-*t*-Bu xerogel	Non-hydrolytic sol–gel synthesis	720	Aminolysis styrene oxide	[74]
$ZrPPAZOSO_3H$	Direct precipitation	47.74	Multi-component reactions	[75]
ZrP mesoporous	Surfactant template EISA (Pluronic P123)	137		[76]
SAxAZP x = 2–20% SA	Sulfamic acid dispersed in micropores of Al-pillared α-ZrP	80–120		[77]
BSA@α-ZrP nanoparticles	Butanesulfonic acid-modified α-ZrP	Particle size 12.61 nm		[78]
ZrP	Reflux, calcination at temp. of 200–600 °C	129.5–79		[79]
α-ZrP	Reflux	33		[80]

Mesoporous zirconium phosphonates with different alkyl chain lengths (ZrHEDP, ZrATMP, and ZrEDTMPS) were obtained in 2015 by Yuan and coworkers through the hydrothermal method in the presence of CTAB [66,67]. The catalysts, which exhibited high surface area and pore volume along with high hydrophobicity proportional to the alkyl chain length, were used in hydrolysis/esterification processes [66] and for chemical CO_2 fixation with aziridine to yield oxazolidinones [67]. The catalytic activity was closely related to hydrophobicity, and ZrHEDP, with the longest alkyl chain, was the best catalyst. Furthermore, it was recovered and reused without significant loss of catalytic activity. This was related to its stable skeletal composition, well-maintained mesoporosity, and high surface area.

In 2017, chemical CO_2 fixation by coupling with epoxides was achieved by Sun and coworkers using $Zr(H_4L)$, a zirconium phosphonate-based metal–organic framework (MOF) [68]. Its performance was higher than that of other MOFs, with no significant loss of catalytic activity after recovery and reuse. The total turnover number (TON) reached as high as 60,000 per mole of catalyst after five runs.

In 2020, porous chromium–zirconium bimetallic phosphates (CrZrP and $CrZr_2P$) were obtained via the sol–gel method by Liu and coworkers [69]. The catalysts were used in the oxidation of cyclohexane, ethylbenzene, and cyclohexene using H_2O_2, TBHP, and O_2, respectively. The high catalytic activity was attributed to the synergistic effect between acidic and Cr^{+6} redox sites, which are influenced by the Cr/Zr molar ratio.

In the same year, Dai and coworkers prepared ZrP loaded on MCM-41 with different ZrP loadings (3–10%) for the oxidative desulfurization of benzothiophene [70]. Under optimal conditions, obtained with 5% ZrP/MCM-41, sulfur removal reached 99.9%. The catalytic activity remained stable for 13 consecutive cycles, and the conversion was still 94.68% in the 14th run. The high catalytic activity was attributed to the high surface area (>600 m^2/g) and surface acid strength.

Zirconium phosphate nanoparticles were obtained in 2021 by Nagaraju and coworkers through a green combustion method using zirconyl nitrate and phosphorous pentoxide as precursors in the presence of tamarind seed powder [71]. The catalyst was used in the microwave-assisted catalytic conversion of aldehydes to nitriles, achieving a high yield (72–98% in 14 examples) with a very low reduction in catalytic activity for up to seven runs. The catalyst was also used in the photocatalytic degradation of dyes, reaching 98% degradation of methylene blue after 150 min of UV irradiation [71].

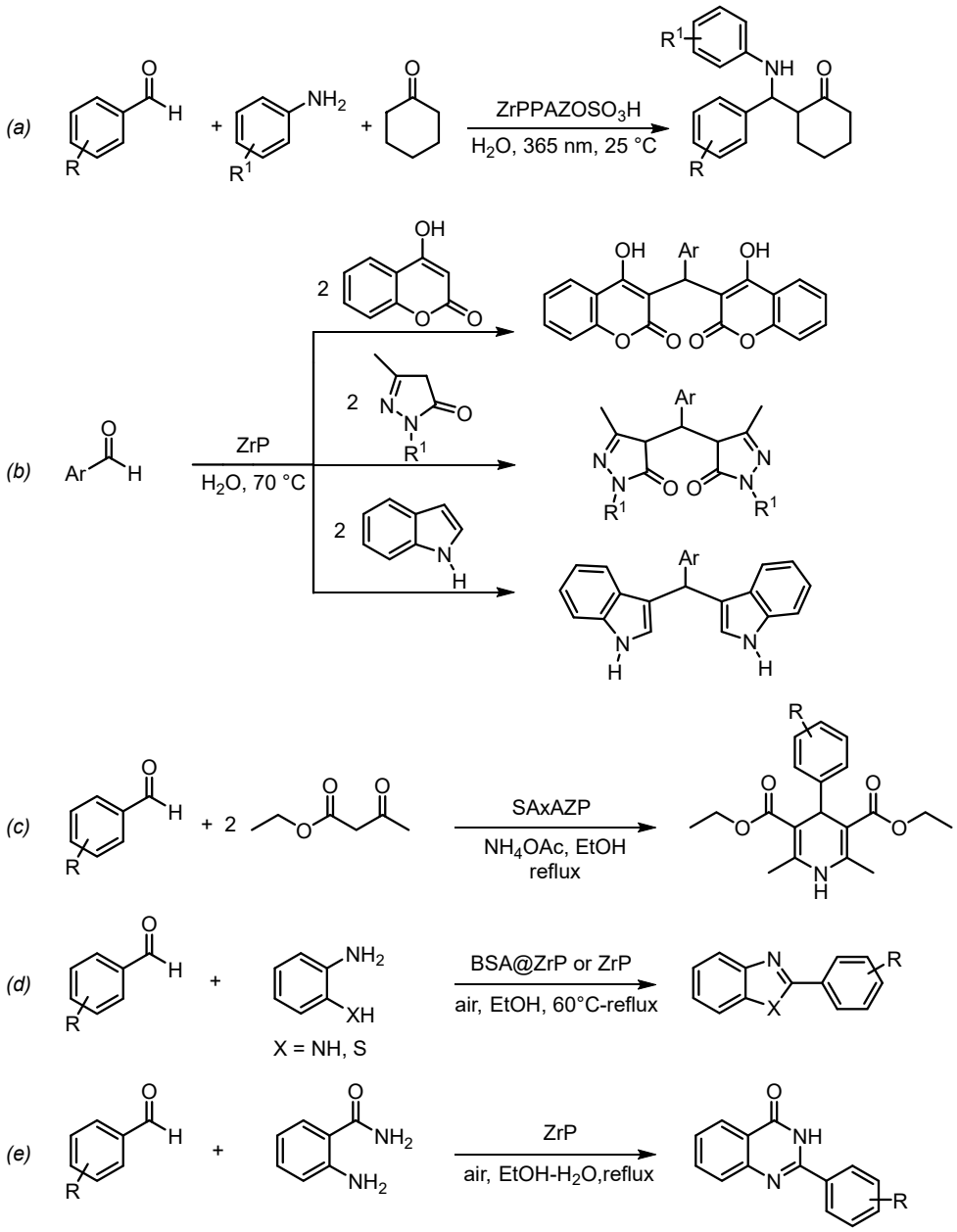
In 2018, Wang and coworkers [72] used three different methods to produce α-ZrP nanoparticles: (1) direct precipitation in the presence of oxalic acid (particle size of 60 nm); (2) the refluxing method (particle size of 47 nm); and (3) the minimal solvent method in polypropylene (particle size of 30 nm). The latter catalysts, having a much smaller crystallite size than the others, were the most active in the photocatalytic degradation of Rhodamine B under ultraviolet irradiation, achieving 97% degradation within 50 min.

In 2022, Biradar and coworkers developed efficient and cost-effective amorphous ZrPs with different P/Zr ratios through refluxing methods for the catalytic valorization of biomass-derived α-Pinene oxide into trans-Carveol, which is used in the fragrance industry to produce essential oil [73]. The solid acid catalyst with a P/Zr ratio of 3 exhibited the highest total acidity and, under optimized reaction conditions, proved to be the best catalyst, resulting in complete conversion with 76% selectivity towards trans-Carveol. The catalyst was recovered and reused up to six times with only a slight loss of activity and selectivity.

In 2023, Pinkas and coworkers obtained zirconium phosphonates with controlled mesoporosity through non-hydrolytic sol–gel synthesis by reacting $Zr(NEt_2)_4$ with trimethylsilylated phosphonates $RP(O)(OSiMe_3)_2$ (R = Me, *t*Bu, Ph, and $OSiMe_3$) and bis-phosphonates $(Me_3SiO)_2(O)P–X–P(O)(OSiMe_3)_2$ (X = CH_2, C_6H_4, $CH_2(C_6H_4)CH_2$, and $CH_2(C_6H_4)_2CH_2$) in dry toluene [74]. The catalytic performance of the prepared xerogels was tested in the aminolysis of styrene oxide with aniline in toluene at 50 °C, and it was closely related to the surface properties. The best performance was achieved with the *t*Bu phosphonate as

the terminal group, which resulted in a higher surface area and porosity, yielding 92% conversion and 94% selectivity.

The acid-catalyzed multi-component reaction (MCR) is one of the most straightforward methods for the synthesis of heterocyclic compounds with important biological and pharmaceutical activities [81]. Typically, MCR is a strategy wherein three or more reaction substrates are combined in a single reaction vessel to form a product via an eco-friendly, step-economical, one-pot cascade fashion. This approach provides the desired product with a usually high yield and high chemo-, regio-, and stereoselectivity, avoiding tedious purification processes. Many examples reported the use of ZrPs as solid acid catalysts for MCRs (Scheme 6).



Scheme 6. ZrP-catalyzed multi-component reactions. Synthesis of (**a**) 2-[aryl(arylamino)methyl]-cyclohexanones; (**b**) aryl bis(heterocyclic)methanes; (**c**) 4-aryl 1,4-dihydropyridines; (**d**) 2-aryl benzimidazoles and benzothiazoles and (**e**) 2-aryl quinazolinones.

In 2016, Chow and coworkers prepared mixed zirconium phosphate–phosphonate by direct precipitation in the presence of 4-[4-(6-phosphonicacid-hexanoxyl)phenylazo] benzenesulfonic acid [75]. The photocontrollable catalyst was used in the one-pot three-component Mannich reaction of benzaldehyde, aniline, and cyclohexanone in water with irradiation at 365 nm (Scheme 6a). High yields and recyclability were obtained for up to seven runs (94.5–91.8% yield). The substituted reactants showed moderate yields (61–78%), which were ascribed to their low solubility in water.

A mesoporous ZrP with high surface area and mesopore volume was obtained through the surfactant template EISA (evaporation-induced self-assembly) method with Pluronic P123 by Karmakar and Saha in 2018 [76]. The catalytic activity was investigated in the tandem Knoevenagel–Michael addition of aromatic aldehydes with different active heterocycles for the preparation of aryl bis(heterocyclic)methanes in water (Scheme 6b). The proposed mechanism involves a Brønsted acid-catalyzed Knoevenagel reaction followed by a Lewis acidic Zr^{4+}-catalyzed Michael addition. The optimized reaction conditions were extended to a large number of substrates, always obtaining high yields (30 examples; 85–97%). Recovery and reuse tests showed good recyclability up to the fourth run.

In 2019, composite organic–inorganic materials (SAxAZP) were obtained through the dispersion of 2–20% sulfamic acid (SA) on a microporous inorganic support of aluminum cluster-pillared α-ZrP (AZP) by Mishra and coworkers [77]. The catalytic activity of the obtained materials was evaluated in the multi-component reaction of ethyl acetoacetate, arylaldehydes/chalcones, and ammonium acetate (Scheme 6c). The composite SA10AZP showed the best catalytic activity, yielding a variety of 1,4-dihydropyridines under mild conditions with high yield and purity (13 examples; 72–90% yield). Lewis acidic Zr^{4+} sites activated aldehyde during the Knoevenagel condensation reaction, while Brønsted acid sites catalyzed the enolization of β-ketoester and the cyclodehydration steps.

The synthesis of 2-aryl benzimidazoles and benzothiazoles was achieved by Khorsandi et al. in 2020 and Sallek et al. in 2023 through a condensation reaction between aldehydes and 1,2-phenylenediamine or 2-aminothiophenol, followed by a successive oxidative aromatization step, under mild conditions and an air atmosphere, using ZrP modified with butanesulfonic acid with the post-grafting method [78], and ZrP was obtained by refluxing and calcination at 200 °C [79], respectively (Scheme 6d). High yields were obtained with both solid acid catalysts, but the latter proved to be more stable, maintaining good catalytic activity for up to five runs [79]. In contrast, butanesulfonic acid-modified ZrP showed a sharp drop in product yield at the fifth run, but no explanation was provided for the loss of catalytic activity [78].

Sallek and coworkers, in 2022 [80], used crystalline α-ZrP, obtained by the refluxing method, as an acid catalyst for the synthesis of 2-arylquinazolinones through a condensation reaction between aldehydes and 2-aminobenzamide in EtOH/H_2O (1:1) as a green reaction medium and in an air atmosphere to promote the oxidative step (Scheme 6e). Excellent yields (89–96%) were obtained whatever the functional group of arylaldehyde. The catalyst was reused five times; a slight decrease was observed due to the accumulation of product on the surface of the catalyst.

4. ZrPs as Solid Base Catalysts

Zirconium phosphonates with basic sites have been less explored than their acidic counterparts; nonetheless, they exhibit interesting catalytic activities (Table 3). The synergistic presence of Zr^{4+} Lewis acid sites and PO_3^{2-} Lewis basic sites on the solid catalyst is often responsible for its remarkable activity.

Table 3. The use of zirconium phosphates as heterogeneous catalysts for base-catalyzed transformation.

Catalyst	Preparation Methods	BET Surface Area m^2/g	Catalyzed Process	Ref.
ZrHEDP ZrEDTMPS ZrATMP ZrDTPMPA	Coprecipitation of phosphonic acid with $ZrOCl_2$ in NaOH	231–108	Levulinic acid and its esters to GVL	[82]
$ZrNPO_3$	Coprecipitation of nitrilotris(methylene)triphophonic acid with $ZrCl_4$	356		[83]
Zr-PhyA porous	Precipitation of phytic acid (PhyA) with $ZrCl_4$	215		[84]
Zr-PhyA porous	Precipitation of phytic acid (PhyA) with $ZrCl_4$	215	MPV reduction in ketones	[84]
α-ZrPK	Potassium-exchanged layered zirconium hydrogen phosphate	17	Multi-component reactions	[85]
ZrP(SIL)	Covalently immobilized ILs on ZrP nanosheet by post-grafting methods	-	Knoevenagel reaction	[86]
ZrPK-Me, ZrPK-Ph, ZrPK-MePh	Potassium-exchanged amorphous zirconium phosphate methyl and/or phenyl phosphonates	42–147		[87]

In 2018, Liu and coworkers prepared hybrid organic–inorganic zirconium phosphonates through the coprecipitation of organic phosphonic acid sodium salt and $ZrOCl_2$ [82]. The solid basic materials exhibited high catalytic activity in the conversion of ethyl levulinate (EL) to γ-valerolactone (GVL) in the presence of isopropanol as a hydrogen donor agent. Phosphonate groups regulate the textural properties and the number of Lewis acid and basic sites, which play a very important role in promoting the conversion of EL to GVL. Indeed, basic sites favor the dissociation of hydroxyl groups in isopropanol, thereby enhancing the rate of the reaction. The catalysts were easily recovered and reused at least five times without any decrease in activity or selectivity.

A zirconium phosphonate ($ZrNPO_3$) with a high surface area (356 m^2/g) and nanoporous structure (average particle size 18 nm) was synthesized in 2022 by Srivastava and coworkers through the coprecipitation of nitrilotris(methylene)triphosphonic acid and $ZrCl_4$ [83]. The catalyst was employed in the selective catalytic hydrogenation of levulinic acid to GVL in the presence of isopropanol as an H-donor, achieving a 98.1% conversion with 98.2% selectivity. The high Lewis acid and basic strength and content of the catalyst were responsible for its high activity and selectivity. The catalyst was highly stable and was reused up to five times with only a slight decrease in conversion and no change in selectivity.

In 2015, Han and coworkers synthesized a porous zirconium phosphonate using natural phytic acid (PhyA) and $ZrCl_4$ as building blocks for the catalytic reduction of levulinic acid and its esters to GVL using isopropanol as H-donor [84]. Also, the excellent catalytic activity (98.7% yield with 98.7% selectivity) was attributed to the properties of both the Zr acid and phosphate basic groups. The catalytic activity and textural properties remained unchanged for up to five cycles. Moreover, the catalyst was used in the Meerwein–Ponndorf–Verley reduction of various carbonyl compounds with very high yields (seven examples; 87.6–99.3%) [84].

In 2016, Rosati and coworkers used potassium-exchanged zirconium hydrogen phosphate, α-$Zr(KPO_4)_2$, as a solid basic catalyst for the preparation of 2-amino-4H-pyran derivatives via a multi-component reaction under solvent-free conditions at 60 °C [85]. A wide variety of pyran derivatives were obtained with high yields (26 examples, 42–93%). The catalyst was reused for up to five runs without loss of catalytic activity.

In 2017, Sun and coworkers [86] prepared an ionic liquid (IL)-modified ZrP single-layer nanosheet by the post-grafting method (ZrP(SiIL)) as a basic solid catalyst for the Knoevenagel condensation reaction of benzaldehyde with ethyl cyanoacetate under solvent free conditions. Thanks to the high level of dispersion, the solid basic catalyst with a ZrP/SiIL ratio of 3 exhibited the highest performance, which was comparable to liquid ionic 1-butyl-3-methylimidazolium chloride (BMIMCl) (99.7 vs. 99.4, respectively). The

catalyst was recovered and reused for up to 11 runs without a significant decrease in catalytic performance.

Amorphous zirconium potassium phosphate methyl and/or phenyl phosphonates were obtained by potassium exchange of the corresponding solid acid by Piermatti and coworkers in 2018 [87]. These organic–inorganic basic solids were tested in the Knoevenagel condensation of various aldehydes with malononitrile or ethyl cyanoacetate under mild, solvent-free conditions. The presence of hydrophobic methyl and phenyl groups on the solid surface affected both the surface properties, favoring the formation of larger pores, and the catalytic activity, enhancing reagent diffusion toward the basic sites and increasing the catalytic activity of the prepared solids compared to completely inorganic layered zirconium potassium phosphate, $Zr(KPO_4)_2$. The mixed zirconium potassium phosphate methyl/phenyl phosphonates (ZrPK-MePh) with higher surface area and pore volume showed the best catalytic activity (nine examples; 89–96% yield). The catalyst was easily recovered by centrifugation and reused for up to five cycles with negligible loss of catalytic activity.

5. ZrPs as Support for Metal Ions and Metal Complex Immobilization

Among the properties that zirconium phosphates exhibit, their high capacity as cation exchangers is extremely useful as it allows for the immobilization of metal ions, which can act as Lewis acid catalysts. The presence of the exchanged metal ions, together with Zr^{4+}, enhances the Lewis acid properties of zirconium phosphates, generally increasing their catalytic activity. Metal complexes can be easily immobilized on the surface of ZrPs layers by the direct intercalation of the metal complex or by flexible ligand methods, which involves first the ion exchange of the metal and then the complexation of the ligand by intercalation. Numerous metal ions and metal complexes have been immobilized on ZrPs by ion exchange, and a selection of these with applications in catalysis is shown in Table 4.

Table 4. Zirconium phosphates as supports for metal ions and metal complex catalyst immobilization and their application in heterogeneous catalysis.

Catalyst	Preparation Methods	BET Surface Area m^2/g	Catalyzed Process	Ref.
ZrP-Cr(III)	Mesoporous zirconium phosphate ion exchange with $CrCl_3$	386	Dehydration of sugar to 5-HMF	[88]
ZrP-Ru(III)	Mesoporous zirconium phosphate ion exchange with $RuCl_3$	378	Oxidation of 5-HMF	[89]
Ru-ZrP	Intercalation of Ru(II) complex into ZrP layers	29	Hydrogenation of furfural to FA Hydrogenation of aldehydes and ketones	[90]
Sn/ZrP	Ultrasonic-assisted impregnation of amorphous ZrP with $SnCl_4$ and calcination at 400 °C	89.1	Isomerization of dihydroxyacetone to lactic acid	[91]
ZrP-Zn	Immobilization of Schiff base Zn(II) complex by covalent grafting on ZrP nanosheet	-	L-lactide polymerization	[92]
ZrP-Zn(II)	Zirconium phosphate ion exchange with $Zn(OAc)_2$	102.4	1,1-diacetate synthesis Oxidation of alcohols	[93] [94]
ZrP-Ni(II)	Zirconium phosphate ion exchange with $Ni(OAc)_2$	103.1	Acetylation of alcohols and phenols	[95]
CoZrP	Ultrasonic-assisted impregnation of Co(II)	146	Hydroformylation of olefins	[96]
α-ZrP/Uracil/Cu(II)	Immobilization of uracil Cu(II) complex by covalent grafting on ZrP nanoparticles	120.1	Morita–Baylis–Hillman C-H functionalization	[97] [78]
NiZrP	Zirconium phosphate ion exchange with $Ni(OAc)_2$	-	Synthesis of tetrazoles	[98]
CuZrP and ZnZrP	Zirconium phosphate ion exchange with $Cu(OAc)_2$ and $Zn(OAc)_2$	-		[99]

Table 4. *Cont.*

Catalyst	Preparation Methods	BET Surface Area m^2/g	Catalyzed Process	Ref.
ZP/xAgCl composite x = 0.28, 0.56, 1.16	Precipitation of AgCl particles by using silver-exchanged nanosized ZrP	AgCl particle size 0.5–2 μm	Photodegradation of dyes	[100]
ZrP-Sn(IV) Sn/Zr = 0.25–1	Zirconium phosphate impregnation with $SnCl_4$	18.3–47.8		[101]
ZrP-Fe(III)	Zirconium phosphate ion exchange with $FeCl_3$	18.56	Oxidation of styrene	[102]
Cu/ZrP	Zirconium phosphate ion exchange with $Cu(OAc)_2$ and calcination at 200 °C	53	Oxidation of phenol	[103]
Cu@ZrDP	Hierarchical porous zirconium phosphonate impregnation with $Cu(NO_3)_2$	408.6	Benzyl alcohol oxidation	[104]
MTO/ZrPP	Impregnation of zirconium phenylphosphonate with methyltrioxyrhenium	-	Epoxidation of alkenes	[105]
ZPS-PVPA·Mn (Salen) ZPS-IPPA·Mn (Salen)	Covalent grafting method	120.3, 100.3		[106]
α-ZrP·Mn (salen)	Flexible ligand method	24.97	Oxidation of cyclohexene	[107]
α-ZrP·M (salen) M = Fe, Mn	Flexible ligand method	18.51, 19.57	Oxidation of cyclohexane	[108]
α-ZrP·M(salicylaldimine) M = Co, Mn, Cu	Covalent bond immobilization of M(salicylaldimine) complex by grafting	5.15–5.18		[109]
ZSPS-PVPA-Mn (Salen)	Zirconium polystyrene phosphonate-supported Salen Mn(III) complex	-	Fixation of CO_2	[110]
ZAMPS-PVPA-Mn (Salen)	Zirconium polystyrene phosphonate-supported Salen Mn(III) complex	-		[111]
10BMIMOAc_Ru-ZrP	Ru(II) complex intercalated into exfoliated α-ZrP modified with BMINOAc	-	Reductive amination of CO_2	[112]

In 2015, Zang and coworkers reported the preparation of mesoporous chromium-exchanged zirconium phosphate with a high surface area (386 m^2/g) for the catalytic conversion of carbohydrates into 5-HMF [88]. Comparing the catalytic activity of ZrP-Cr(III) with that of simple mesoporous ZrP (98.5% vs. 6.1% fructose conversion), the authors concluded that Cr^{3+} was the active site promoting the dehydration of fructose. The Cr-catalyst was very stable: the yield of 5-HMF remained almost stable for six consecutive runs, the Cr valence remained trivalent, and no Cr leaching was detected in the solution.

In 2016, the same authors obtained a Ru(III) ion-exchanged mesoporous ZrP for the oxidation of biomass-derived 5-HMF [89]. A 100% conversion of HMF at 130 °C after 12 h under atmospheric oxygen pressure was achieved, and 2,5-furandicarboxylic acid (FDCA) and 2,5-diformylfuran (DFF) were detected as the major oxidation products. The ZrP–Ru(III) catalyst was recovered and reused for up to five cycles without any loss of catalytic activity.

In 2021, Hou and coworkers immobilized the cationic Ru(II) complex [(*p*-cymene)Ru(phen)Cl]Cl by intercalation into the interlayer space of exfoliated α-ZrP and investigated its catalytic activity in the selective hydrogenation of furfural and other carbonyl compounds to the corresponding alcohols under mild conditions [90]. High catalytic performance was obtained for a wide variety of carbonyl compounds (15 examples; 83–99% conversion with 25–99% selectivity), and the catalyst was easily recycled for six runs with good catalytic activity. The remarkable performance was attributed, through DFT calculations, to the coordination interaction of the Ru(II) center with the P-OH groups within the ZrP interlayers. This interaction led to the formation of Ru-O bonds, which activated and dissociated H_2, enabling the selective hydrogenation of carbonyl groups. Moreover,

suitable interlayer spacing and appropriate exfoliation were crucial for immobilizing the Ru complex and favoring the formation of the active Ru-O species.

In 2023, a Sn-doped zirconium phosphate was obtained by Ju and coworkers through the ultrasonic-assisted impregnation of amorphous ZrP with $SnCl_4$ and successive calcination for the isomerization of dihydroxyacetone to lactic acid in water as the solvent [91]. The authors proved that the presence of Sn significantly increased the content of strong Lewis acid sites, which accelerated the conversion of pyruvaldehyde to lactic acid. The catalyst was reused for up to four runs without significant loss of catalytic performance and with very low ion leaching.

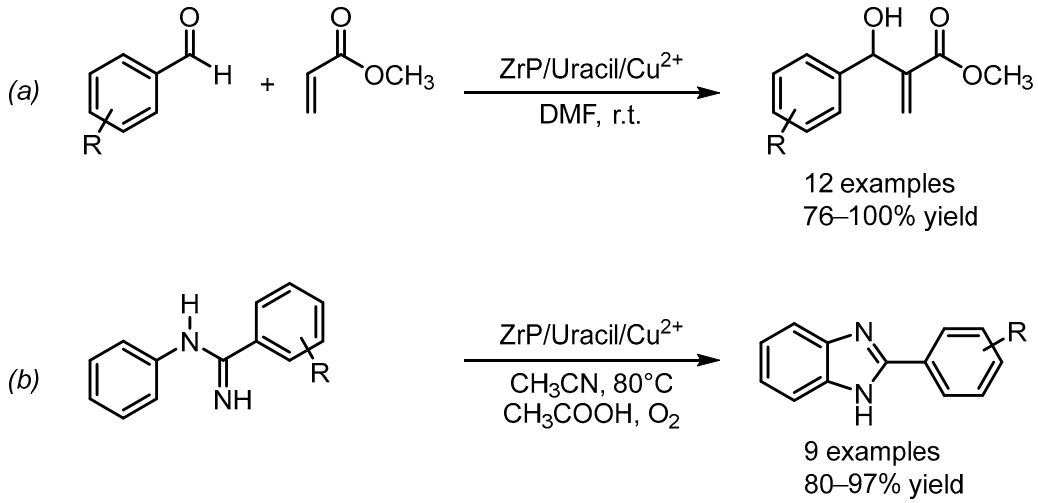
The polymerization of L-lactide to polylactide-based nanocomposite was achieved by Sun and coworkers in 2019 by using an α-ZrP nanosheet-supported zinc catalyst obtained through the immobilization of a Schiff base Zn(II) complex by covalent grafting [92]. The prepared ZrP−Zn catalyst promoted the polymerization of lactide and subsequently acted as a nanofiller for the polylactide matrix, improving its crystallization behavior and mechanical properties.

In 2015, Karimi prepared zinc zirconium phosphate nanoparticles with a high surface area (102.4 m^2/g) by ion exchange with $Zn(OAc)_2$. The catalyst was used for the chemoselective synthesis of 1,1-diacetates by reacting aldehydes with acetic anhydride [93] and for the selective oxidation of a wide range of alcohols to their corresponding ketones or aldehydes using H_2O_2 as an oxidant [94], both under mild and solvent-free conditions. High yields were observed, and the catalyst was recovered and reused for several runs. A slight decrease in catalytic activity was observed after several cycles due to Zn^{2+} leaching from the ZrP surface and catalyst agglomeration after thermal regeneration. The reduction in Lewis acid sites reduced the catalytic performance.

In 2016, nickel zirconium phosphate nanoparticles were obtained by Hajipour and coworkers through ion exchange with $Ni(OAc)_2$ [95]. The catalyst was used for the acetylation of a wide range of phenols, alcohols, thiols, and amines with acetic anhydride, achieving good to excellent yields under solvent-free conditions (36 examples; 81–96% yield). The nanocatalyst was recovered and reused for at least seven runs, with a slight decrease in catalytic activity being observed after the sixth run due to particle agglomeration and Ni leaching into the solution.

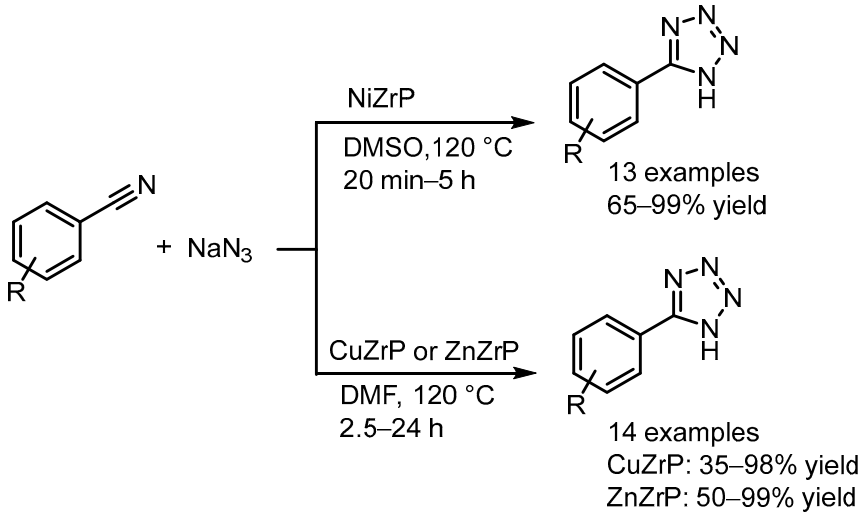
The catalytic hydroformylation of olefins to the corresponding aldehydes over single-atom Co(II) sites in zirconium phosphate (CoZrP), obtained by the ultrasonic-assisted impregnation of $Co(NO_3)_2$ on amorphous ZrP, was reported by Hou and coworkers in 2022 [96]. The excellent performance and high stability of the Co(II)-based catalyst for six consecutive catalytic recycles were attributed to strong coordination interactions between single-atom Co(II) sites and the phosphate groups on ZrP, which improved the catalytic performance and stability by preventing Co(II) leaching.

In 2018, Hajipour and coworkers immobilized a uracil Cu(II) complex by covalent grafting on the surface of α-ZrP nanoparticles [97]. The catalyst was used in the Morita–Baylis–Hillman reaction of methyl acrylate, 2-cyclopentenone, or acrylamide with aryl aldehydes (Scheme 7a) [97]. The catalytic cycle involved the activation of the α,β-unsaturated substrate by uracil organocatalysis, while the Cu^{2+} Lewis acid center activated the process through interaction with carbonyl groups. Later, in 2020, the same catalyst was used for the synthesis of benzimidazoles via the Cu^{2+}-catalyzed C–H functionalization of benzamides (Scheme 7b) [78]. The catalyst was reused for seven runs in both examples. A slight decrease in activity was observed until the fourth cycle, but a significant drop occurred thereafter, despite the recovered catalyst maintaining its textural properties and showing no leaching.



Scheme 7. Catalytic activity for α-ZrP/Uracil/Cu^{2+}. (**a**) Morita-Baylis-Hillman reaction; (**b**) Synthesis of 2aryl benzoimidazoles.

Abrishami and coworkers prepared nickel [98], copper, and zinc zirconium phosphate nanocatalysts [99] through α-ZrP ion exchange with the corresponding metal acetate for the synthesis of 5-substituted-1*H*-tetrazoles via the [3+2] cycloaddition between various nitriles and sodium azide (Scheme 8). CuZrP and ZnZrP worked well in DMF as the solvent, showing good catalytic activity (35–99% yield; 2.5–24 h) [99], while NiZrP exhibited higher catalytic activity using DMSO as the solvent, resulting in high yields (13 examples; 65–99%) in shorter reaction times (20 min–5 h) [98]. The interactions of nitrogen atoms of nitrile and azide with the metal ions accelerate the cycloaddition step compared to simple ZrP. The catalysts were recovered and reused for five runs, showing only a slight decrease at the fifth cycle.



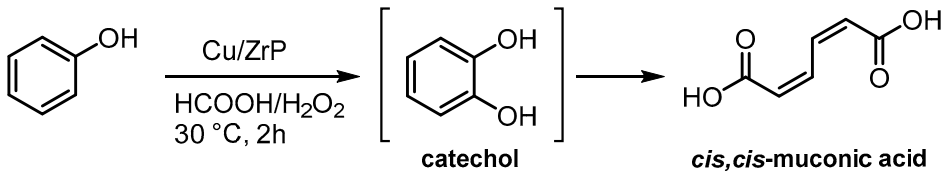
Scheme 8. Synthesis of tetrazole over Ni, Cu, and ZnZrP.

In 2015, Casciola and coworkers prepared ZP/xAgCl composites with different amounts of AgCl by reacting hydrochloric acid with silver-exchanged nanosized ZrP samples [100]. The catalytic activity of the ZP/AgCl composites was tested in the photodegradation of Rhodamine B under UV irradiation with a halogen lamp at room temperature. The composite ZP/1.16AgCl was the best photocatalyst, achieving complete chromophore degradation within 15 min. Moreover, the photocatalyst was recovered and reused for three runs, achieving the complete degradation of Rhodamine B in 10 min by the third catalytic cycle, which is significantly faster than the fresh catalyst.

Tin-doped α-ZrPs with different Sn/Zr ratios (0.25–1) were obtained through the impregnation of crystalline zirconium phosphate with $SnCl_4$ by Harmalani and coworkers in 2021 [101]. The textural properties of the materials were affected by the addition of Sn, showing a decrease in crystallinity and increases in surface area and pore volume, which contribute to their catalytic activity. The materials were tested in the photocatalytic degradation of dyes, and a significant increase in catalytic activity was observed with the increasing amount of tin.

The oxidation of styrene was achieved by Khare and coworkers in 2015 using iron-exchanged zirconium phosphate, ZrP-Fe(III), under solvent-free conditions with tert-butyl hydroperoxide as an oxidant [102]. In the best conditions, benzaldehyde (84.75% selectivity) and styrene oxide (10.85% selectivity) with a conversion of 28.81% were obtained after 5 h. The catalyst retained its textural properties and catalytic activity for up to three runs.

In 2023, Hou and coworkers achieved the selective oxidation of phenol into the highly valuable platform molecule, *cis*,*cis*-muconic acid, using copper-exchanged ZrP and in situ-generated performic acid under mild reaction conditions (30 °C; 2 h) (Scheme 9) [103]. The authors demonstrated that α-ZrP exhibited preferential selectivity towards dihydroxybenzene, while the Cu(II)-O-P linkage in α-ZrP-supported copper catalysts was the catalytically active species for the further oxidative cleavage of catechol to *cis*,*cis*-muconic acid (66% conversion with 60% selectivity). Moreover, the strong Cu(II)-O-P interaction endowed the catalyst with high stability and recyclability for up to four runs. However, a drop in selectivity (from 60% to 50%) was observed in the fifth cycle due to a reduction in the copper content (from 4% to 3.2%).



Scheme 9. ZrP-supported copper catalyst for selective oxidation of phenol to *cis*,*cis*-muconic acid.

Hierarchical porous zirconium phosphonate with a multi-nitrogen heterocyclic structure (ZrDP) was synthesized by Xu and coworkers in 2024 [104]. This porous material, with a high surface area (408.6 m^2/g) and strong metal coordination ability, was used to immobilize Cu(II), Fe(III), and Co(II) metal ions. The Cu@ZrDP composite exhibited excellent catalytic activity in the selective oxidation of benzyl alcohol to benzaldehyde in DMF at 80 °C for 8 h using air as the sole oxidant (67.7% conversion; 90.2% selectivity). Recovery and reuse tests showed stable catalytic efficiency for up to five cycles. These results, along with the hot filtration test, confirmed the high stability of the composite, which was attributed to the strong coordination of the metal ions with the multi-nitrogen heterocyclic structure in the ZrDP framework.

The epoxidation of olefins to epoxides is a crucial process in fine chemical manufacturing, providing essential building blocks for pharmaceuticals, agrochemicals, and epoxy resins. Developing efficient, environmentally benign, and recoverable catalysts for this reaction remains a significant research challenge. In 2015, Zhang and coworkers immobilized a methyltrioxorhenium complex (MTO) on the surface of zirconium phenylphosphonate (MTO/ZrPP) using a conventional impregnation method for the epoxidation of cyclohexene [105]. Excellent catalytic activity and selectivity were obtained under mild conditions using urea–hydrogen peroxide as the oxidant (92.2% yield with 100% selectivity). Filtration tests and DFT calculations revealed that MTO is strongly anchored to the support surface through favored hydrogen bonding interactions between the two oxo ligands of MTO and two hydrogen atoms from the adjacent phenyl groups of ZrPP.

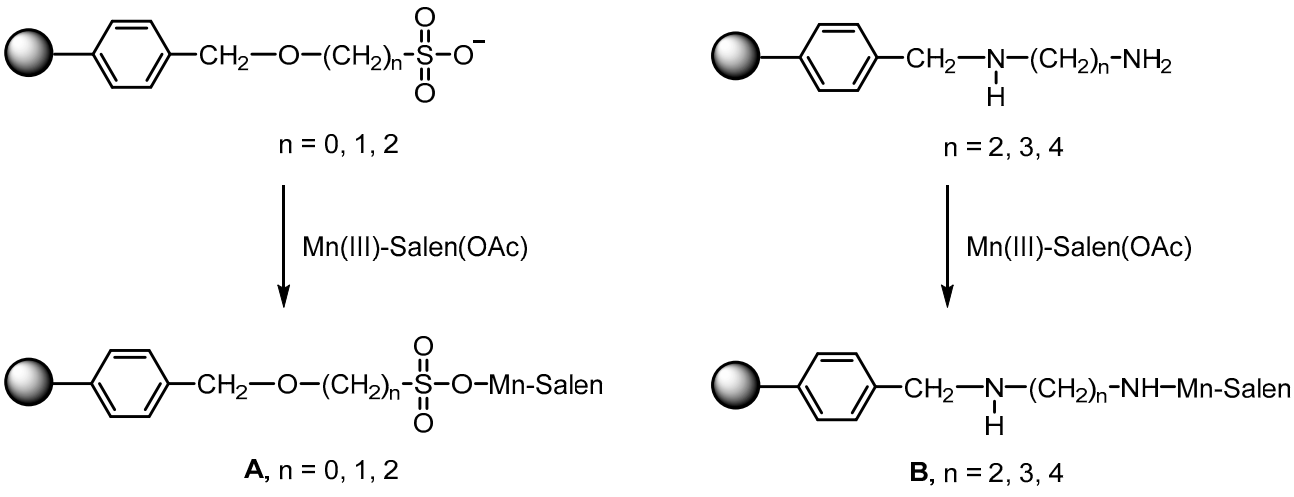
The asymmetric epoxidation of alkenes was achieved by Zou and coworkers in 2017 by immobilizing a chiral MnIII(salen) complex on modified zirconium poly(styrene-phenylvinylphosphonate) (ZPS-PVPA) and zirconium poly(styrene-isopropenyl phospho-

nate) (ZPS-IPPA) through the covalent grafting method [106]. The supported catalyst ZPS-PVPA-Mn-Salen, with a larger pore diameter and surface area, was found to be more active than the ZPS-IPPA-based catalyst and showed higher chiral induction (ee 83%) compared to the corresponding homogeneous catalyst (ee 54%) for the asymmetric epoxidation of α-methylstyrene using NaClO as the oxidant. The catalysts were recycled for up to 11 runs, with only a slight decrease in activity observed until the eighth cycle. However, a drop in reactivity and selectivity was observed thereafter.

Metal–Salen intercalated α-ZrP catalysts (α-ZrP·M (Salen), where M = Mn(II) and Fe(III)) were synthesized in situ by Khare and coworkers using zirconium phosphate ion exchange with $Mn(OAc)_2$ or $FeCl_3$, followed by intercalation with Salen using the flexible ligand method [107,108]. In 2016, the authors tested the activity of α-ZrP·Mn (Salen) for the catalytic oxidation of cyclohexene using tert-butyl hydroperoxide (TBHP) as the oxidant [107]. Under optimized conditions (conversion 85.5%), cyclohexenone was obtained as the major product (67.8% selectivity). Moreover, the catalytic system was reused for three runs with negligible loss of activity. In 2017, the authors used the Mn(II) and Fe(III) materials for the oxidation of cyclohexane with TBHP [108]. It was found that the reactivity of α-ZrP·Fe (Salen) was greater than its analogous Mn(II), achieving a conversion of 29.30% and a selectivity for the cyclohexanol/cyclohexanone mixture (KA oil) of 97.20%. Additionally, α-ZrP·Fe (Salen) was recycled for five runs, maintaining stable activity until the third cycle, with a slight drop observed thereafter.

In 2016, Khare and Shrivastava immobilized transition metal–salicylaldimine complexes onto the α-ZrP surface through covalent grafting (α-ZrP·M(salicylaldimine), where M = Co, Mn, and Cu) for the oxidation of cyclohexane with TBHP [109]. The best result was obtained with α-ZrP·Co(salicylaldimine), which showed a conversion of 14.18% and a KA oil selectivity of 92.33%. No leaching of Co was detected, and stable catalytic activity was observed for five runs.

In 2019, Lu and coworkers prepared two Mn-based catalysts, ZSPS-PVPA-Salen Mn(III) (**A**) and ZAMPS-PVA-Salen Mn(III) (**B**) (Scheme 10), for CO_2 fixation by cycloaddition to propylene oxide [110,111]. The Mn(II)–Salen complex was immobilized on organic–inorganic zirconium polystyrene phosphonates with different carbon chains and different organic groups (SO_3^- or NH_2) (Scheme 10). The best catalytic activity was obtained with catalyst **A** with n = 2, achieving a conversion of 95.8% at 120 °C for 4 h. Additionally, the catalyst was used in the cycloaddition of CO_2 to various epoxides, consistently showing high conversion and selectivity (four examples; 90.9–94.2% conversion with 90.7–96.1% selectivity) and was recycled for seven runs. A slight decrease in activity was observed due to Mn-complex decomposition under cycloaddition conditions.



Scheme 10. Zirconium polystyrene phosphonate-supported Salen–Mn(II) complex, ZSPS-PVPA-Salen Mn(III) (**A**) and ZAMPS-PVA-Salen Mn(III) (**B**).

In 2024, Hou and coworkers developed a Ru(II) complex intercalated into exfoliated α-ZrP, modified with the ionic liquid BMINOAc, for the N-formylation of amines with CO_2 and H_2 under biphasic reaction conditions [112]. Studies indicated that the reaction occurred within the ZrP interlayers, where CO_2, H_2, and amine molecules were simultaneously activated, enhancing the reaction rate through reactant enrichment. The ionic liquid not only facilitated the further exfoliation of ZrP but also promoted amine enrichment in the interlayer via hydrogen bonding interactions. Meanwhile, CO_2 molecules benefited from the synergistic effect between the imidazolium cation and the phosphate groups of ZrP. Furthermore, the Ru(II) complex intercalated into exfoliated ZrP (10BMINOAc_Ru-ZrP catalyst) exhibited significantly higher activity compared to crystalline ZrP (Ru-α-ZrP), highlighting that exfoliation and intercalation were crucial for achieving high catalytic efficiency. This method was successfully applied to a range of aliphatic amines (nine examples; 90–96% conversion and 99% selectivity), though it was less effective for the formylation of aniline (16% conversion). The catalytic system was successfully recovered and reused, maintaining stable activity even after seven cycles.

6. ZrPs as Supports for Metal NPs and Metal Oxide NPs Immobilization

Metal nanoparticles (MNPs), with their high surface-to-volume ratio, are widely utilized in various fields, including bio-diagnostics, medicine, drug delivery, pharmacology, energy production, and environmental remediation [113–116]. They are also effective as catalytic systems, facilitating a range of chemical transformations such as C–C coupling, reduction, and oxidation reactions [117–124]. The efficiency of these nanocatalysts is highly dependent on factors like nanoparticle size and shape, the stabilizing ligands used, and the nature of the support material. The immobilization and stabilization of MNPs on solid supports are of particular interest in heterogeneous catalysis, as this approach is key to achieving sustainability, high activity, and recyclability. Suitable supports are chosen to prevent particle migration and aggregation, which can reduce catalytic efficiency. Additionally, the solid matrix enhances catalytic performance by ensuring a homogeneous distribution of active sites and minimizing catalyst leaching. In this context, layered zirconium phosphate and phosphonates, with their high surface area, chemical and thermal stability, tunable structural features, and high capacity as cation exchangers, offer attractive support for metal nanoparticles. The immobilization process typically involves ion exchange with the metal cation, followed by its reduction to metal nanoparticles. Examples of both precious and non-precious MNPs immobilized on ZrPs and their catalytic applications are presented in Table 5.

Table 5. Zirconium phosphates as supports for metal NP and metal oxide NP immobilization and their application in heterogeneous catalysis.

Catalyst	Preparation Methods	MNPs Size	Catalyzed Process	Ref.
Ni/ZrP	Exfoliated ZrP ion exchange with $Ni(NO_3)_2$ and reduction with H_2 flow at 400 °C	30.3 nm	Hydrodeoxygenation of 5-HMF	[125]
Ni/ZrP	Impregnation with $Ni(NO_3)_2$, calcination, and reduction with H_2 flow at 550 °C	-	Depolymerization of lignin	[126]
Pd@ZrP	Impregnation with $Pd(NO_3)_2$ and calcination	11.9 nm		[127]
Ru/CoO/ZrP	Impregnation with $Co(NO_3)_2$ and calcination followed by impregnation with $RuCl_3$, calcination, and reduction	-	Hydrogenolysis of glycerol	[128]
Pt/7WOx-ZrP	Impregnation of tungsten modified ZrP with $H_2PtCl_6\cdot$, calcination, and reduction	3–6 nm		[129]

Table 5. *Cont.*

Catalyst	Preparation Methods	MNPs Size	Catalyzed Process	Ref.
WOx/ZrP	Impregnation with Na_2WO_4 and calcination at 300 °C	-	Alcoholysis of polylactic acid	[130]
NiZrP2	Impregnation with $Ni(NO_3)_2$ and reduction with H_2 flow at 400 °C	20 nm	Hydrolysis/hydrogenation of cellulose	[131]
Co/ZrP and Ni/ZrP	Impregnation, calcination, and reduction with H_2 flow at 500 °C	5 nm, 29 nm	Hydrodeoxygenation of lignin derivatives	[132]
Ni/ZrP	Impregnation with $Ni(NO_3)_2$, calcination, and reduction with H_2 flow at 550 °C	20.74 nm		[133]
2V/ZrP-m	Mechanochemical synthesis and calcination at 550 °C	<4 nm	Glycerol oxidation to formic acid	[134]
Ru-ZrP	Ion exchange with $RuCl_3$ and microwave-assisted reduction	3.14 nm	Hydrogenation of acetophenone	[135]
CdS QD@ZrP	Ion exchange with $Cd(OAc)_2$ followed by treatment with Na_2S	2–6 nm	Photocatalytic oxidation of benzyl alcohol	[136]
ZrP-Ti	TiO_{2-x} cluster grafted on ZrP nanosheet via chemical bonding with P element	2–5 nm	Photodegradation of dyes	[137]
Pd@ZPGly	Impregnation with $Pd(OAc)_2$	2–5 nm	Suzuki reactions	[138,139]
Pd@MZrP	Impregnation with $Pd(OAc)_2$ and reduction with $NaBH_4$	7–8 nm		[140]
Pd@ZrCP	Impregnation with $Pd(OAc)_2$ and reduction with $NaBH_4$	5 nm		[141]
PdNP/α-ZrPK	Impregnation with $Pd(OAc)_2$ in EtOH	5–15 nm	Heck reactions	[142]
Pd@ZPGly	Impregnation with $Pd(OAc)_2$	2–5 nm		[139]
Pd@ZrP	Adsorption of $Pd(NH_3)_4Cl_2$ and reduction with $NaBH_4$	3–7 nm		[143]
Pd@ZPGly	Impregnation with $Pd(OAc)_2$	2–5 nm	Nitroarenes reduction	[144]
Au@ZP(AEP)	Impregnation with $HAuCl_4$ and reduction with $NaBH_4$	7.8 ± 2.4 nm		[145]
ZrP-SH(Au)	Impregnation with $HAuCl_4$ and reduction with $NaBH_4$	2 ± 1 nm		[146]
Au/ZrP composite	Impregnation with $HAuCl_4$ and reduction with Na-citrate	15 nm		[147]
Ag@C/ZrPP	Ion exchange with $[Ag_{74}(C{\equiv}CPh)_{44}](NO_3)_2$ cluster, carbonization, calcination, and reduction	1–2 nm		[148]
ZrP@PDA/Ag	Ag^+ impregnation and in situ reduction on ZrP nanosheets coated with polydopamine	29.6 nm		[149]
ZrP@PDA/Au	Au^{3+} impregnation and in situ reduction on ZrP nanosheets coated with polydopamine	6.5 nm		[150]
Ag/ZrP	Impregnation with $AgNO_3$, calcination, and reduction with $NaBH_4$	6.5 nm		[151]
Pt/ZrP	Impregnation with H_2PtCl_2 and reduction with H_2 flow at 200 °C	8–11 nm		[152]
Pt/ZrP	Adsorption of $Pt(NH_3)_4Cl_2$ on ZrP nanosheet and annealing at 400 °C under air	1.4 ± 0.3 nm	NOx reduction	[153]

In 2018, Liu and coworkers prepared Ni nanoparticles immobilized on exfoliated ZrP through ion exchange with $Ni(NO_3)_2$, followed by calcination and reduction under H_2 flow at a high temperature [125]. TEM images revealed Ni particles with an average size of about 30 nm on the α-ZrP layers. The catalytic activity of Ni/ZrP was tested in the hydrodeoxygenation of 5-HMF to 2,5-dimethylfuran (DMF). The synergistic effect of metallic Ni and Zr^{4+} Lewis acidic sites from α-ZrP support was favorable for the hydrogenolysis of C−OH groups of HMF, achieving a 100% conversion of HMF and a 68.1% yield of DMF at 240 °C and 5 MPa H_2 over 20 h. The catalyst retained its activity for up to five runs.

In 2019, Li and coworkers achieved the depolymerization of lignin via a hydrogenolysis process using NiNPs supported on zirconium phosphate by using isopropanol as both the hydrogen donor and solvent under 2 MPa H_2 at 260 °C [126]. The synergistic effect between the Lewis and Brønsted acids of ZrP facilitated significant hydrogen production, while metallic Ni acted as the active center for catalytic hydrogenolysis. The amount of Ni was crucial for effective lignin depolymerization, with the yields of phenolic monomers increasing as Ni loading increased; 15% Ni(0) loading resulted in the highest conversion and selectivity. Moreover, this material is reusable, maintaining satisfactory lignin conversion and para-ethylphenol yield even after four consecutive runs.

Very recently, Singh and coworkers achieved the depolymerization of poplar lignin residue, derived from cholinium lysinate ([Ch][Lys]) ionic liquid-based biorefinery, into guaiacols using a zirconium phosphate-supported palladium catalyst [127]. This catalyst was prepared by impregnating ZrP with $Pd(NO_3)_2$, followed by calcination. High conversion (>80%) and a high yield of guaiacols, up to 200 mg per g of lignin, were obtained along with good reusability of the nanocatalyst for up to four runs.

In 2020, Hou and coworkers developed a zirconium phosphate-supported Ru/CoO bimetallic catalyst for the direct hydrogenolysis of glycerol to propanal in a continuous flow reactor at 270 °C and 2 MPa H_2 [128]. The Brønsted acid sites on ZrP were crucial for the dehydration of glycerol into acrolein, while the cooperative effect of Ru(0) sites and finely dispersed CoO species facilitated the selective hydrogenation of the conjugated C=C bond in acrolein, yielding propanal. The catalyst achieved full glycerol conversion and 80.2% selectivity for propanal, with high stability for at least 50 h of long-term performance. Additionally, the catalyst could be regenerated for reuse simply by calcining in air to remove carbonaceous deposits.

In the same year, the same authors investigated the effect of tungsten modification on a zirconium phosphate-supported Pt catalyst for the selective hydrogenolysis of glycerol to 1-propanol in a continuous flow reactor at 270 °C and 2 MPa H_2 [129]. The incorporation of WOx species increased the total acidity, enhanced the dehydration of glycerol into acrolein, and improved the dispersion of PtNPs, which facilitated H_2 dissociation and subsequent hydrogenation to 1-propanol. The nanocatalyst achieved full glycerol conversion, yielding 81% of 1-propanol over at least 70 h of continuous reaction, and it could be regenerated by calcination in air.

Very recently, Chen and coworkers synthesized amorphous ZrP-supported WOx active sites with high surface area and enhanced acidity through impregnation with Na_2WO_4 and calcination at 300 °C for 4 h [130]. The resulting 10% WOx/ZrP catalyst showed excellent activity in the methanol alcoholysis of polylactic acid (PLA) to produce methyl lactate (MLA), which can be further converted to lactide, thus enabling a sustainable process for the chemical upcycling of end-of-life plastics. The MLA yield reached 94.5% within 4 h at 160 °C, outperforming traditional solid acids due to the abundance of WOx active sites and strong acidity. Additionally, the 10% WOx/ZrP catalyst demonstrated versatility in the alcoholysis of discarded PLA-based products and was reusable for at least five cycles.

The direct synthesis of hexitols from microcrystalline cellulose and birch over zirconium phosphate-supported NiNPs nanocatalysts was reported by Zhang and coworkers in 2021 [131]. The study highlighted that the match between the acidity of the ZrP support, modulated by the P/Zr ratio, and the hydrogenation activity of NiNPs was crucial to inhibit humin formation and enhance sorbitol production from cellulose. The optimal catalyst was

Ni/ZrP2 (P/Zr = 2), with a Ni loading of 20%, that allowed for a 60.8% yield of sorbitol to be obtained when microcrystalline cellulose was used as the substrate under 5 MPa H_2 at 200 °C in 5 h.

In 2019, Lee and coworkers reported the catalytic hydrodeoxygenation of lignin-derived guaiacol to cyclohexane using Co/ZrP and Ni/ZrP catalysts at 573 K and 70 bar H_2 [132]. The study identified two distinct reaction pathways via major intermediates: (i) the 2-methoxycyclohexanol route, involving the hydrogenation of guaiacol with Ni/ZrP, where cyclopentanemethanol and methylcyclopentane byproducts were also observed, and (ii) the phenol route, involving the demethoxylation of guaiacol with Co/ZrP, which resulted in a high cyclohexane yield (76%).

Similarly, the catalytic hydrodeoxygenation of lignin-derived vanillin to 2-methoxy-4-metilphenol, using a nickel-supported ZrP catalyst at 220 °C and 0.5 MPa H_2, was reported by Zhang and coworkers in 2022 [133]. Compared to various metal phosphates (TiP, NbP, LaP, and CeP), Ni/ZrP showed the highest activity, attributed to its small Ni particle size (20.74 nm), large specific surface area, optimal acidity, and strong metal–support interaction. The Lewis acid sites on ZrP promoted vanillin adsorption and activation, Brønsted acid sites favored dehydration, and Ni nanoparticles facilitated H_2 dissociation. A high vanillin conversion of 97.25% and an 88.39% yield of 2-methoxy-4-methylphenol were achieved in 30 min. The catalyst also demonstrated good recyclability, with no significant activity loss up to the fourth cycle.

In 2019, Hou and coworkers developed a zirconium phosphate-supported vanadium catalyst through mechanochemical synthesis followed by calcination (2V/ZrP-m) [134]. This catalyst showed high catalytic activity for glycerol oxidation to formic acid by using O_2 (3 MPa) as the terminal oxidant in an aqueous medium at 170 °C. The process achieved high glycerol conversion (85.6%) and formic acid yield (53.5%), with good reusability for up to five cycles. The vanadium species (primarily V^{5+}), with an average size of less than 4 nm, were highly dispersed and exhibited strong interactions with the ZrP support, enhancing both the activity and stability of the catalyst. Additionally, a synergistic effect was observed between the Lewis acid sites of the ZrP support, which facilitated glycerol activation, and the vanadium species, which were responsible for glycerol dehydrogenation and subsequent oxidation to formic acid.

In 2020, Zhang and coworkers reported the preparation of small-sized Ru nanoparticles immobilized on α-ZrP nanoplatelets through ion exchange followed by microwave-assisted reduction [135]. This catalyst was applied in the hydrogenation of acetophenone, where it demonstrated significantly improved catalytic performance compared to pure α-ZrP nanoplatelets. The Ru-ZrP catalyst achieved full conversion of acetophenone under 4 MPa H_2 at room temperature within 2 h, with a yield of 1-cyclohexylethanol reaching up to 95%. The catalyst maintained its activity over five recycling runs, with only a slight decrease observed in the fifth cycle.

In 2022, Gogoi and coworkers utilized α-ZrP as a crystalline support for CdS quantum dots [136]. The resulting composite, featuring CdS quantum dots with an average size in the range of 2–6 nm homogeneously dispersed over α-zirconium phosphate, was tested for its photocatalytic performance in the oxidation of benzyl alcohol to benzaldehyde in acetonitrile under visible light irradiation. The photocatalyst achieved a 90% conversion with 99% selectivity and maintained its efficiency for up to five cycles. Only a slight decrease in performance was observed thereafter, attributed to catalyst decomposition, as evidenced by FT-IR spectra and powder X-ray diffraction patterns.

In 2015, Liu and coworkers immobilized TiO_{2-x} clusters with an average particle size in the range of 2–5 nm using a modified post-grafting method via chemical bonding with the P element on both faces of α-ZrP nanosheets (ZrP–Ti) [137]. The obtained nanocomposites showed enhanced visible light absorption properties compared to pure TiO_2, resulting in improved photocatalytic activities in the photodegradation of methylene blue under solar irradiation. The best catalytic performance was obtained over ZrP–Ti with the P/Ti molar ratio of 1:1, achieving a degradation efficiency of 100%. This improvement was attributed

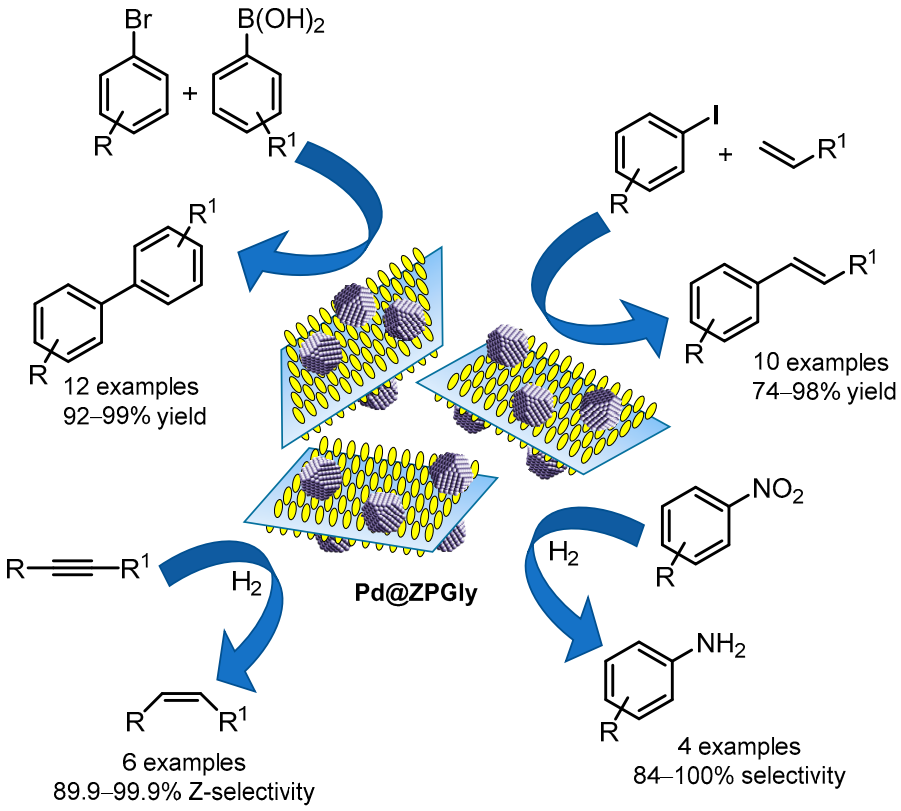
to the highly accessible TiO_{2-x} clusters and the enhanced optical properties resulting from the P doping effects.

Palladium nanoparticles (PdNPs) have garnered significant attention due to their unique electronic and chemical properties, making them highly efficient as heterogeneous nanocatalysts for various organic transformations [117]. Among these, Pd-catalyzed carbon–carbon (C-C) coupling reactions, such as the Suzuki–Miyaura and Heck reactions, are particularly noteworthy and extensively applied in the synthesis of natural products, agrochemicals, pharmaceutical intermediates, and materials science. Despite their advantages, a key challenge in using PdNPs lies in their recoverability and reusability, as well as minimizing metal leaching, given palladium's precious nature. To address these challenges, supporting PdNPs on stable materials has become an effective strategy to enhance catalytic activity, stability, and ease of recovery. Among various supports, layered zirconium phosphates (ZrPs) have emerged as promising candidates. Their high surface area, chemical stability, and tunable properties provide an excellent platform for stabilizing PdNPs, preventing aggregation, and ensuring a uniform distribution of active sites, thereby enhancing the overall catalytic performance in C-C coupling reactions [11].

In 2015, Nocchetti, Vaccaro, and coworkers prepared a zirconium phosphate–carboxya minophosphonate nanosheet (ZPGly) through exfoliation with propylamine in water [138]. The stable colloidal dispersion of single sheets was used as a support for the immobilization of Pd nanoparticles through impregnation with $Pd(OAc)_2$ for 15 days. This process resulted in the homogeneous dispersion of Pd nanoparticles on the sheet surfaces with an average size of 2 nm (Pd@ZPGly). The catalytic activity of this nano-material was first tested in the Suzuki–Miyaura coupling of phenylboronic acid and aryl bromides, performed in a flow reactor at 70 °C using ethanol (EtOH 96%) as the solvent and K_2CO_3 as the base. The products were isolated with high yields (96–98%) simply by removing the solvent under reduced pressure. The catalyst was reused for three consecutive runs, consistently yielding the desired product with a 97% yield and negligible Pd leaching (3–5 ppm). In 2017, the same authors compared the catalytic activity of different Pd@ZPGly samples obtained by contacting ZPGly dispersion with palladium acetate solutions for 1, 7, and 15 days in the Suzuki–Miyaura reaction under both batch and flow conditions [139]. The best catalyst, Pd@ZPGly-15, used in low amounts (0.1 mol % Pd), demonstrated the highest catalytic activity and the lowest Pd leaching across a wide range of substrates (12 examples; 92–99% yield) (Scheme 11). Moreover, the sustainability of the protocol was significantly improved by using the heterogeneous K_2CO_3/EtOH 96% system, as no purification step was required (E-factor 27.7 in batch). This value was notably reduced in a large-scale flow protocol by recovering the ethanol reaction medium through distillation (E-factor 3.2).

In 2018, Gogoi and coworkers developed a Pd catalyst for Suzuki–Miyaura cross-coupling reactions by immobilizing Pd nanoparticles on mesoporous zirconium organo-phosphonates through the impregnation of $Pd(OAc)_2$, followed by reduction with $NaBH_4$ [140]. The resulting nanocatalyst (Pd@MZrP) featured palladium nanoparticles with an average size of 7–8 nm, homogeneously dispersed on the zirconium phosphonate framework. The catalyst exhibited good yields for a wide range of substrates (12 examples; 22–92% yield) and maintained its effectiveness for up to five runs with only a slight decrease in yield.

The same authors also developed an efficient catalyst for the Suzuki–Miyaura cross-coupling reaction by immobilizing Pd nanoparticles onto a layered zirconium carboxyphosphonate support through impregnation with $Pd(OAc)_2$, followed by reduction with $NaBH_4$ [141]. The resulting catalyst (Pd@ZrCP) featured mixed-valent Pd(0)/Pd(II) nano-sized aggregates with an average size of 5 nm, homogeneously distributed over the zirconium carboxyphosphonate framework. Under optimized reaction conditions, the catalyst provided very high catalytic activity, characterized by an exceptionally short reaction time of 2 min and a high turnover frequency of $1.3 \times 10^4\ h^{-1}$. Additionally, the catalyst exhibited excellent recyclability, maintaining its performance for up to five runs with no detectable Pd leaching in either the isolated reaction products or the reaction medium.



Scheme 11. Catalytic application of Pd@ZPGly in C-C coupling and reduction reactions.

A clean Heck reaction, catalyzed by palladium nanoparticles immobilized on layered potassium zirconium phosphate (PdNP/α-ZrPK) in a CH_3CN/H_2O azeotrope as a green recoverable medium, with triethylamine as the base at 120 °C, was reported by Piermatti, Vaccaro, and coworkers in 2015 [142]. High yields were achieved in batch conditions for the Heck reaction of methyl acrylate and styrene with various aryl iodides (17 examples; 67–99%). To further enhance the experimental procedures and catalyst efficiency, the process was optimized under flow conditions by using polystyrene-supported triethylamine (PS-TEA), allowing for the isolation of the final product without any purification step, resulting in a very low residual palladium content (6 ppm) and extremely low waste production (E-factor 4.6).

In 2017, the same authors compared the catalytic activity of PdNP/α-ZrPK with Pd@ZPGly, which had already been used as a catalyst in the Suzuki–Miyaura reaction, in the Heck coupling reaction (Scheme 11) [139]. The reactions were conducted in a CH_3CN/H_2O azeotrope as a green, recoverable medium, with TEA as the base at 120 °C for 3 h. The catalyst exhibited high catalytic activity, and the products were isolated in high yield (10 examples, 74–98%). When the Heck reaction was performed in a flow reactor using PS-TEA as the base, an extremely low Pd content (2 ppm) was detected. This result highlighted the remarkable ability of phosphate–carboxyaminophosphonate groups present on the surface of the nanosheets to stabilize Pd nanoparticles. Moreover, the catalyst retained its catalytic activity over six consecutive runs.

In 2022, Tong and coworkers obtained Pd nanoparticles supported on α-zirconium phosphate nanosheets as catalysts for the Heck reaction of methyl acrylate with aryl iodide in dimethylformamide (DMF) as the solvent, with Et_3N as the base at 100 °C for 20 min–3 h [143]. The Pd@ZrP nanocatalyst exhibited excellent catalytic activity, achieving a TOF value of 937.3 h^{-1} when iodobenzene and methylacrylate were used as substrates. In addition, the catalyst was easily recovered by centrifugation and reused for up to six runs without a significant decrease in catalytic activity, although a drop was observed thereafter.

The reduction of nitroaromatics is a crucial reaction in the synthesis of fine chemicals, serving as a key step in the production of a wide range of valuable compounds, including anilines and azo- and azoxy-compounds, which are important intermediates in the manufacture of pharmaceuticals, agrochemicals, dyes, and polymers [154–157]. The ability to perform this reaction under mild conditions with high selectivity is of great significance as it contributes to the development of more sustainable and environmentally friendly chemical processes. Accordingly, numerous procedures have been developed for the reduction of nitroaromatic compounds which use supported metal nanoparticles [158–162]. Among these, zirconium phosphate and phosphonate-supported metal nanoparticles, primarily Pd, Au, Ag, and Pt, have been widely used for the selective reduction of nitroarenes (Table 5).

In 2018, Liguori utilized Pd@ZPGly, prepared using 20% of the ion exchange capacity of propylamine and with a low Pd loading, for the hydrogenation of nitroarenes in methanol solution at room temperature and 5 bar of H_2 (Scheme 11) [144]. High conversion and good selectivity were observed across a variety of nitroarenes (4 examples; 84–100% selectivity), with complete dehalogenation achieved for 4-bromonitrobenzene. The catalyst was also employed for the selective hydrogenation of alkynes, achieving high TOF and excellent selectivity towards the desired Z-alkene (Z-sel. 89.9–99.9%) (Scheme 11). Stable catalytic activity was maintained upon recycling, with negligible metal leaching into the solution.

A large number of reports highlight the use of ZrP-supported Au nanoparticles for the selective reduction of nitroarenes. In 2019, Pica, Piermatti, Vaccaro, and coworkers reported the use of a zirconium phosphate aminoethyl phosphonate, ZP(AEP), bearing aminoethyl groups on the layer surface, to immobilize AuNPs with an average size of 7.8 nm [145]. The gold-based catalyst proved to be effective for the chemoselective and switchable reduction of nitroarenes to their corresponding azoxyarenes or anilines, simply by performing the reaction in 96% ethanol or absolute ethanol, respectively, by using $NaBH_4$ as a reducing agent. Good to excellent yields were obtained for a wide variety of nitroaromatics, and stable catalytic activity was obtained over five runs. Moreover, the reactions were optimized under flow conditions to define a simpler and greener protocol for obtaining the two possible products. An increase in the efficiency and stability of the catalyst, with very low Au leaching, was observed when switching from batch to flow conditions, attributed to the stable packing inside the reactor.

In the same years, Sun and coworkers [146] and Chung and coworker [147] obtained AuNPs immobilized on ZrP nanosheets modified by grafting with γ-propyl mercaptotrimethoxysilane (ZrP-SH) and N^1-(3-trimethoxysilylpropyl)diethylenetriamine (A-ZrP), respectively. These supported AuNP nanocomposites were used as effective catalysts for the reduction of 4-nitrophenol to aminophenol in water, with the reaction progress monitored through UV-vis absorption spectroscopy, using $NaBH_4$ as the reductant. Although the gold nanoparticles on the thiol-functionalized ZrP (ZrP-SH/Au) were much smaller than those on the amino-functionalized ZrP (Au/A-ZrP) (2 nm vs. 15 nm), the latter exhibited significantly higher activity, achieving complete conversion in just 180 s at room temperature. Furthermore, the catalyst maintained its performance over 10 cycles with negligible loss of catalytic activity.

Zirconium pyrophosphate-supported Ag nanoclusters, with a very small size of 1–2 nm, were developed by Chen and coworkers in 2019 [148]. The preparation involved the intercalation of α-ZrP with the $[Ag_{74}(C{\equiv}CPh)_{44}](NO_3)_2$ cluster, followed by carbonization, calcination, and reduction under H_2. The resulting catalyst, Ag@C/ZrPP, was tested in the hydrogenation of a series of nitroaromatics in tetrahydrofuran under 4 MPa H_2 pressure. The catalyst demonstrated high yields of aniline derivatives and excellent recyclability, maintaining performance over six cycles with very low Ag leaching. The zirconium pyrophosphate support not only stabilized the Ag clusters but also enhanced the adsorption/activation of nitroarene substrates through its strong Brønsted and Lewis acid sites.

Xu and coworker utilized α-ZrP nanosheets coated with polydopamine (PDA) to immobilize silver NPs [149], and in a more recent study, they used gold NPs [150] through

impregnation and the in situ reduction of Ag^{+} or Au^{+3}. The resulting ZrP@PDA/Ag nanocatalyst featured AgNPs with an average size of 29.6 nm, while the ZrP@PDA/Au catalyst exhibited smaller AuNPs with a particle size of 6.5 nm. The catalytic activity of these catalysts was evaluated through UV-vis absorption spectroscopy in the reduction of 4-nitrophenol into 4-aminophenol in water by using $NaBH_4$ as a reducing agent. The TOF achieved by ZrP@PDA/Au was as high as 38.10 min^{-1}, which is higher than that for ZrP@PDA/Ag (TOF 32.36 m^{-1}) and significantly higher than that of some reported noble metal-based catalysts. Moreover, ZrP@PDA/Au showed high stability and reusability for up to five runs.

In 2023, Hou and coworkers prepared ZrP-supported AgNPs with an average size of 6.5 nm through wet impregnation with $AgNO_3$, followed by calcination and subsequent reduction [151]. The catalyst exhibited high catalytic activity in the hydrogenation of nitroarenes to azoxybenzene compounds in MeOH, using $NaBH_4$ as a hydrogen source. High yields and selectivity were achieved at room temperature in very short reaction times (3–20 min) for a variety of nitroarenes. Furthermore, the Ag/ZrP catalyst was recycled eight times with a negligible loss of activity, and no leaching of Ag species was observed. The high activity was attributed to the surface acidic sites of ZrP, which not only stabilized the highly dispersed AgNPs but also facilitated the adsorption and activation of the substrates.

In the same years, Hou immobilized platinum NPs with an average size of 8–11 nm on the surface of amorphous ZrP through wetness impregnation with H_2PtCl_2, followed by reduction with H_2 flow [152]. The catalyst exhibited high catalytic performance in the selective hydrogenation of nitrobenzene to *p*-aminophenol. A full conversion of nitrobenzene and high selectivity to *p*-aminophenol (89%) were achieved in the presence of inorganic acid and dimethylsulfoxide (DMSO) as cosolvents in water at 80 °C and 0.6 MPa H_2. Moreover, the catalyst was reused for 14 consecutive runs without a significant decrease in activity and selectivity. It was demonstrated that the nitro functional group was adsorbed on acid sites of zirconium phosphate and reduced to *N*-phenylhydroxylamine by active hydrogen on Pt(0) sites, followed by acid-site-catalyzed rearrangement to afford *p*-aminophenol.

In 2024, Machida and coworkers synthesized platinum nanoparticles (PtNPs) with an average size of 1.4 nm by adsorbing $Pt(NH_3)_4Cl_2$ onto ZrP nanosheets, followed by annealing at 400 °C for 3 h under air [153]. This catalytic system was successfully applied in the selective catalytic reduction of NO_X at 150 °C under H_2/O_2/He atmosphere. The 0.49 wt% Pt/ZrP nanosheets exhibited high NO conversion (89%) and good N_2 selectivity (83%), and the recovered catalyst maintained its catalytic activity over three cycles. Further investigation indicated that the small Pt particles, combined with a high loading of Pt on the ZrP nanosheet structure, were crucial for achieving a high NO conversion rate while minimizing NO_X byproduct formation.

7. Conclusions

The exploration of zirconium phosphates and phosphonates (ZrPs) in heterogeneous catalysis has revealed their versatility and effectiveness in enhancing catalytic processes. Through careful adjustment of their structural and surface properties, ZrPs have been shown to significantly impact the efficiency, selectivity, and sustainability of various catalytic reactions. As catalysts or supports, they offer robust platforms for the dispersion and stabilization of active species with the added benefit of facilitating catalyst recovery and reuse. This makes them not only valuable in current applications but also promising candidates for future advancements in green chemistry. The continued research and development of ZrPs and their derivatives are expected to contribute substantially to the evolution of more sustainable and efficient catalytic systems.

Author Contributions: Conceptualization and writing—original draft preparation, O.P. Writing, review and editing, A.D., M.P., M.N. and O.P. All authors have read and agreed to the published version of the manuscript.

Funding: This research was funded by the European Union—NextGenerationEU under the Italian Ministry of University and Research (MUR) National Innovation Ecosystem grant ECS00000041—VITALITY—CUP J97G22000170005. The University of Perugia is acknowledged for providing financial support to the university project "Fondo Ricerca di Ateneo, edizione 2022".

Conflicts of Interest: The authors declare no conflicts of interest.

References

1. Thomas, J.M.; Thomas, W.J. (Eds.) *Principles and Practice of Heterogeneous Catalysis*; Wiley-VCH: Weinheim, Germany, 1996.
2. Schlögl, R. Heterogeneous catalysis. *Angew. Chem. Int. Ed.* **2015**, *54*, 3465–3520. [CrossRef] [PubMed]
3. Hagen, J. *Industrial Catalysis: A Practical Approach*, 3rd ed.; Wiley-VCH: Weinheim, Germany, 2015.
4. Mallesham, B.; Raikwar, D.; Shee, D. The role of catalysis in green synthesis of chemicals for sustainable future. In *Advanced Functional Solid Catalysts for Biomass Valorization*; Elsevier: Amsterdam, The Netherlands, 2020; Chapter 1, pp. 1–37. [CrossRef]
5. Pálinkó, I. Heterogeneous catalysis: A fundamental pillar of sustainable synthesis. In *Green Chemistry*; Elsevier: Amsterdam, The Netherlands, 2018; Chapter 3.12, pp. 415–447. [CrossRef]
6. Vaccaro, L.; Curini, M.; Ferlin, F.; Lanari, D.; Marrocchi, A.; Piermatti, O.; Trombettoni, V. Definition of green synthetic tools based on safer reaction media, heterogeneous catalysis, and flow technology. *Pure Appl. Chem.* **2018**, *90*, 21–33. [CrossRef]
7. Friend, C.M.; Xu, B. Heterogeneous catalysis: A central science for a sustainable future. *Acc. Chem. Res.* **2017**, *50*, 517–521. [CrossRef]
8. Chatterjee, R.; Bhanja, P.; Bhaumik, A. The design and synthesis of heterogeneous catalysts for environmental applications. *Dalton Trans.* **2021**, *50*, 4765–4771. [CrossRef]
9. Torok, B.; Schaefer, C.; Kokel, A. *Heterogeneous Catalysis in Sustainable Synthesis*; Elsevier: Amsterdam, The Netherlands, 2021.
10. Zhu, Y.P.; Ren, T.Z.; Yuan, Z.Y. Insights into mesoporous metal phosphonate hybrid materials for catalysis. *Catal. Sci. Technol.* **2015**, *5*, 4258–4279. [CrossRef]
11. Pica, M. Zirconium phosphate catalysts in the XXI century: State of the art from 2010 to date. *Catalysts* **2017**, *7*, 190. [CrossRef]
12. Li, D.; Ni, W.; Hou, Z. Conversion of biomass to chemicals over zirconium phosphate-based catalysts. *Chin. J. Catal.* **2017**, *38*, 1784–1793. [CrossRef]
13. Xiao, H.; Liu, S. Zirconium phosphate (ZrP)-based functional materials: Synthesis, properties and applications. *Mater. Des.* **2018**, *155*, 19–35. [CrossRef]
14. Ramos-Garcés, M.V.; Colón, J.L. Preparation of zirconium phosphate nanomaterials and their applications as inorganic supports for the oxygen evolution reaction. *Nanomaterials* **2020**, *10*, 822. [CrossRef]
15. Lv, X.W.; Weng, C.C.; Zhu, Y.P.; Yuan, Z.Y. Nanoporous Metal Phosphonate Hybrid Materials as a Novel Platform for Emerging Applications: A Critical Review. *Small* **2021**, *17*, 2005304. [CrossRef]
16. Yadav, S.; Beniwal, N.; Rekha, P.; Singh, L. Recent advances in the synthesis and applications of porous zirconium phosphate. *J. Porous Mater.* **2022**, *29*, 1707–1725. [CrossRef]
17. Amghouz, Z.; García, J.R.; Adawy, A. A Review on the Synthesis and Current and Prospective Applications of Zirconium and Titanium Phosphates. *Eng* **2022**, *3*, 161–174. [CrossRef]
18. Rathore, K.; Jangir, R. Insight into Synthesis, properties and applications of metal Phosphonates: Emphasis on catalytic activities. *Inorg. Chim. Acta* **2024**, *559*, 121804. [CrossRef]
19. Vivani, R.; Costantino, F.; Taddei, M. Zirconium phosphonates. In *Metal Phosphonate Chemistry*; Clearfield, A., Demadis, K.D., Eds.; The Royal Society of Chemistry: London, UK, 2011; Chapter 2, pp. 45–86. [CrossRef]
20. Bashir, A.; Ahad, S.; Malik, L.A.; Qureashi, A.; Manzoor, T.; Dar, G.N.; Pandith, A.H. Revisiting the old and golden inorganic material, zirconium phosphate: Synthesis, intercalation, surface functionalization, and metal ion uptake. *Ind. Eng. Chem. Res.* **2020**, *59*, 22353–22397. [CrossRef]
21. Pica, M.; Donnadio, A.; Casciola, M. From microcrystalline to nanosized α-zirconium phosphate: Synthetic approaches and applications of an old material with a bright future. *Coord. Chem. Rev.* **2018**, *374*, 218–235. [CrossRef]
22. Bisio, C.; Brendlé, J.; Cahen, S.; Feng, Y.; Hwang, S.J.; Melanova, K.; O'Hare, D.; Rabu, P.; Leroux, F. Recent Advances and Perspectives for Intercalation Layered Compounds Part 1: Design and applications in the field of energy. *Dalton Trans.* **2024**, *53*, 14525–14550. [CrossRef]
23. Bisio, C.; Brendle, J.; Cahen, S.; Feng, Y.; Hwang, S.J.; Nocchetti, M.; O'Hare, D.; Rabu, P.; Melanova, K.; Leroux, F. Recent Advances and Perspectives for Layered Intercalation Compounds Part 2: Applications in the field of catalysis, environment and health. *Dalton Trans.* **2024**, *53*, 14551–14581. [CrossRef]
24. Ramos-Garcés, M.V.; Sanchez, J.; La Luz-Rivera, K.; Del Toro-Pedrosa, D.E.; Jaramillo, T.F.; Colón, J. LMorphology control of metal-modified zirconium phosphate support structures for the oxygen evolution reaction. *Dalton Trans.* **2020**, *49*, 3892–3900. [CrossRef] [PubMed]
25. Alberti, G.; Casciola, M.; Vivani, R.; Biswas, R.K. Preparation and characterization of zirconium phosphate phosphonates, $ZrPO_4(H_2PO_4)_{1-x}(RPO_2OH)_x \cdot nH_2O$, with γ-layer structure (R = CH_3, C_3H_7, C_6H_{11}). *Inorg. Chem.* **1993**, *21*, 4600–4604. [CrossRef]
26. Cheng, Y.; Wang, X.; Jaenicke, S.; Chuah, G.K. Minimalistic Liquid-Assisted Route to Highly Crystalline α-Zirconium Phosphate. *ChemSusChem* **2017**, *10*, 3235–3242. [CrossRef]

27. Cheng, Y.; Chui, S.S.Y.; Wang, X.D.T.; Jaenicke, S.; Chuah, G.K. One-pot synthesis of layered disodium zirconium phosphate: Crystal structure and application in the remediation of heavy-metal-contaminated wastewater. *Inorg. Chem.* **2019**, *58*, 13020–13029. [CrossRef] [PubMed]
28. Cheng, Y.; Zhang, H.; Jaenicke, J.A.; Tan, E.C.; Chuah, G.K. Minimalistic synthesis of α-zirconium diammonium phosphate and zirconia for applications in ion exchange and catalysis. *ACS Sustain. Chem. Eng.* **2019**, *7*, 895–904. [CrossRef]
29. Bevara, S.; Giri, P.; Patwe, S.J.; Achary, S.N.; Mishra, R.K.; Kumar, A.; Sinha, A.K.; Kaushik, C.P.; Tyagi, A.K. Separation of ^{90}Sr from nuclear waste by crystalline complex phosphates of Ce (IV) and Zr (IV). *J. Environ. Chem. Eng.* **2018**, *6*, 2248–2261. [CrossRef]
30. Tarafdar, A.; Panda, A.B.; Pradhan, N.C.; Pramanik, P. Synthesis of spherical mesostructured zirconium phosphate with acidic properties. *Microporous Mesoporous. Mater.* **2006**, *95*, 360–365. [CrossRef]
31. Sun, Y.; Afanasiev, P.; Vrinat, M.; Coudurier, G. Porous zirconium phosphates prepared by surfactant-assisted precipitation. *J. Mater. Chem.* **2000**, *10*, 2320–2324. [CrossRef]
32. Chakraborty, R.; Bhattacharaya, K.; Chattopadhyay, P. Nanostructured zirconium phosphate as ion exchanger: Synthesis, size dependent property and analytical application in radiochemical separation. *Appl. Radiat. Isot.* **2014**, *85*, 34–38. [CrossRef]
33. Zhu, Y.; Kanamori, K.; Moitra, N.; Kadono, K.; Ohi, S.; Shimobayashi, N.; Nakanishi, K. Metal zirconium phosphate macroporous monoliths: Versatile synthesis, thermal expansion and mechanical properties. *Microporous Mesoporous Mater.* **2016**, *225*, 122–127. [CrossRef]
34. Alberti, G.; Casciola, M.; Marmottini, F.; Vivani, R. Preparation of mesoporous zirconium phosphate-pyrophosphate with a large amount of thermally stable acid groups on the pore surface. *J. Porous Mater.* **1999**, *6*, 299–305. [CrossRef]
35. Lanari, D.; Montanari, F.; Marmottini, F.; Piermatti, O.; Orrù, M.; Vaccaro, L. New zirconium hydrogen phosphate alkyl and/or aryl phosphonates with high surface area as heterogeneous Brønsted acid catalysts for aza-Diels–Alder reaction in aqueous medium. *J. Catal.* **2011**, *277*, 80–87. [CrossRef]
36. Angeloni, M.; Piermatti, O.; Pizzo, F.; Vaccaro, L. Synthesis of Zirconium Phosphonate Supported L-Proline as an Effective Organocatalyst for Direct Asymmetric Aldol Addition. *Eur. J. Org. Chem.* **2014**, *2014*, 1716–1726. [CrossRef]
37. Ding, H.; Ahmed, A.; Shen, K.; Sun, L. Assembly of exfoliated α-zirconium phosphate nanosheets: Mechanisms and versatile applications: Nanoscience: Special Issue Dedicated to Professor Paul S. Weiss. *Aggregate* **2022**, *3*, e174. [CrossRef]
38. Jain, A.; Shore, A.M.; Jonnalagadda, S.C.; Ramanujachary, K.V.; Mugweru, A. Conversion of fructose, glucose and sucrose to 5-hydroxymethyl-2-furfural over mesoporous zirconium phosphate catalyst. *Appl. Catal. A Gen.* **2015**, *489*, 72–76. [CrossRef]
39. Xu, H.; Miao, Z.; Zhao, H.; Yang, J.; Zhao, J.; Song, H.; Liang, N.; Chou, L. Dehydration of fructose into 5-hydroxymethylfurfural by high stable ordered mesoporous zirconium phosphate. *Fuel* **2015**, *145*, 234–240. [CrossRef]
40. Antonetti, C.; Melloni, M.; Licursi, D.; Fulignati, S.; Ribechini, E.; Rivas, S.; Parajó, J.C.; Cavani, F.; Raspolli Galletti, A.M. Microwave-assisted dehydration of fructose and inulin to HMF catalyzed by niobium and zirconium phosphate catalysts. *Appl. Catal. B Environ.* **2017**, *206*, 364–377. [CrossRef]
41. Saravanan, K.; Park, K.S.; Jeon, S.; Bae, J.W. Aqueous phase synthesis of 5-hydroxymethylfurfural from glucose over large pore mesoporous zirconium phosphates: Effect of calcination temperature. *ACS Omega* **2018**, *3*, 808–820. [CrossRef]
42. Zhu, C.; Cai, C.; Liu, Q.; Li, W.; Tan, J.; Wang, C.; Chen, L.; Zhang, Q.; Ma, L. Continuous Production of 5-Hydroxymethylfurfural from Monosaccharide over Zirconium Phosphates. *ChemistrySelect* **2018**, *3*, 10983–10990. [CrossRef]
43. Ni, W.; Li, D.; Zhao, X.; Ma, W.; Kong, K.; Gu, Q.; Chen, M.; Hou, Z. Catalytic dehydration of sorbitol and fructose by acid-modified zirconium phosphate. *Catal. Today* **2019**, *319*, 66–75. [CrossRef]
44. Cao, D.; Yu, B.; Zhang, S.; Cui, L.; Zhang, J.; Cai, W. Isosorbide production from sorbitol over porous zirconium phosphate catalyst. *Appl. Catal. A Gen.* **2016**, *528*, 59–66. [CrossRef]
45. Zhu, Y.; Kanamori, K.; Brun, N.; Pélisson, C.H.; Moitra, N.; Fajula, F.; Hulea, V.; Galarneau, A.; Takeda, K.; Nakanishi, K. Monolithic acidic catalysts for the dehydration of xylose into furfural. *Catal. Commun.* **2016**, *87*, 112–115. [CrossRef]
46. Kumar, A.; Srivastava, R. Zirconium Phosphate Catalyzed Transformations of Biomass-Derived Furfural to Renewable Chemicals. *ACS Sust. Chem. Eng.* **2020**, *8*, 9497–9506. [CrossRef]
47. Zhai, P.; Lv, G.; Cai, Z.; Zhu, Y.; Li, H.; Zhang, X.; Wang, F. Efficient Production of Ethyl Levulinate from Furfuryl Alcohol Catalyzed by Modified Zirconium Phosphate. *ChemistrySelect* **2019**, *4*, 3940–3947. [CrossRef]
48. Li, W.; Li, M.; Liu, H.; Jia, W.; Yu, X.; Wang, S.; Zeng, X.; Sun, Y.; Wei, J.; Tang, X.; et al. Domino transformation of furfural to γ-valerolactone over SAPO-34 zeolite supported zirconium phosphate catalysts with tunable Lewis and Brønsted acid sites. *Mol. Catal.* **2021**, *506*, 11538. [CrossRef]
49. He, J.; Liu, X.; Bai, L.; Liu, S.; Song, K.; Zhou, X.; Guo, J.; Meng, X.; Li, C. Effective one-pot tandem synthesis of γ-valerolactone from biogenic furfural over zirconium phosphate catalyst. *Biofuels Bioprod. Biorefin.* **2022**, *16*, 1613–1626. [CrossRef]
50. Li, F.; France, L.J.; Cai, Z.; Li, Y.; Liu, S.; Lou, H.; Long, J.; Li, X. Catalytic transfer hydrogenation of butyl levulinate to γ-valerolactone over zirconium phosphates with adjustable Lewis and Brønsted acid sites. *Appl. Catal. B Environ.* **2017**, *214*, 67–77. [CrossRef]
51. Dookheh, M.; Najafi Chermahini, A.; Saraji, M. Preparation of Alkyl Levulinates from Xylose Over Modified Bifunctional Mesoporous Zirconium Phosphate Catalysts. *Catal. Lett.* **2022**, *152*, 2141–2154. [CrossRef]
52. Jamali, F.; Chermahini, A.N.; Ayashi, N. Conversion of Levulinic Acid to n-Butyl Levulinate over Mesoporous Zirconium Phosphate Catalysts. *Inorg. Chem. Res.* **2021**, *5*, 149–162. [CrossRef]

53. Rocha, G.O.; Lopes, F.S. Esterification of levulinic acid over tetravalent metal phosphates: An efficient route to fuel additives. *Catal. Today* **2024**, *442*, 114905. [CrossRef]
54. Kasipandi, S.; Cho, J.M.; Park, K.S.; Shin, C.H.; Wook Bae, J. Unprecedented activity and stability on zirconium phosphates grafted mesoporous silicas for renewable aromatics production from furans. *J. Catal.* **2020**, *385*, 10–20. [CrossRef]
55. Wu, C.; Wu, T.; Li, J.; Liu, C.L.; Dong, W.S. Highly efficient catalytic conversion of biomass-derived 2,5-dimethylfuran into renewable p-xylene over zirconium phosphate catalysts. *Appl. Catal. A Gen.* **2023**, *663*, 119323. [CrossRef]
56. Zhou, Y.; Noshadi, I.; Ding, H.; Liu, J.; Parnas, R.S.; Clearfield, A.; Xiao, M.; Meng, Y.; Sun, L. Solid acid catalyst based on single-layer α-Zirconium phosphate nanosheets for biodiesel production via esterification. *Catalysts* **2018**, *8*, 17. [CrossRef]
57. Pan, H.; Xia, Q.; Li, H.; Wang, Y.; Shen, Z.; Wang, Y.; Li, L.; Li, X.; Xu, H.; Zhou, Z.; et al. Direct production of biodiesel from crude Euphorbia lathyris L. Oil catalyzed by multifunctional mesoporous composite materials. *Fuel* **2022**, *309*, 122172. [CrossRef]
58. Wang, M.; Yang, H.; Xie, Y.; Wu, X.; Chen, C.; Ma, W.; Dong, Q.; Hou, Z. Catalytic transformation of glycerol to 1-propanol by combining zirconium phosphate and supported Ru catalysts†. *RSC Adv.* **2016**, *6*, 29769–29778. [CrossRef]
59. Srinivasa Rao, G.; Hussain, S.; Chary, K.V.R. Porous zirconium phosphate solid acid catalysts with variable Zr/P ratio for gas phase glycerol dehydration to acrolein. *Mater. Today Proc.* **2018**, *5*, 25773–25781. [CrossRef]
60. Testa, M.L.; La Parola, V.; Mesrar, F.; Ouanji, F.; Kacimi, M.; Ziyad, M.; Liotta, L.F. Use of zirconium phosphate-sulphate as acid catalyst for synthesis of glycerol-based fuel additives. *Catalysts* **2019**, *9*, 148. [CrossRef]
61. Jiang, Y.; Zhou, R.; Zhao, H.; Ye, B.; Long, Y.; Wang, Z.; Hou, Z. A highly active and stable organic-inorganic combined solid acid for the transesterification of glycerol under mild conditions. *Chin. J. Catal.* **2021**, *42*, 1772–1781. [CrossRef]
62. Li, X.; Jiang, Y.; Zhou, R.; Hou, Z. Layered α-zirconium phosphate: An efficient catalyst for the synthesis of solketal from glycerol. *Appl. Clay Sci.* **2019**, *174*, 120–126. [CrossRef]
63. Li, X.; Jiang, Y.; Zhou, R.; Hou, Z. Acetalization of glycerol with acetone over appropriately-hydrophobic zirconium organophosphonates. *Appl. Clay Sci.* **2020**, *189*, 105555. [CrossRef]
64. Zou, X.; Nie, X.; Tan, Z.; Shi, K.; Wang, C.; Wang, Y.; Zhao, X. Synthesis of sulfonic acid-functionalized zirconium poly(Styrene-phenylvinyl-phosphonate)-phosphate for heterogeneous epoxidation of soybean oil. *Catalysts* **2019**, *9*, 710. [CrossRef]
65. Agarwal, B.; Kailasam, K.; Sangwan, R.S.; Elumalai, S. Traversing the history of solid catalysts for heterogeneous synthesis of 5-hydroxymethylfurfural from carbohydrate sugars: A review. *Renew. Sust. Energy Rev.* **2018**, *82*, 2408–2425. [CrossRef]
66. Lin, X.Z.; Ren, T.Z.; Yuan, Z.Y. Mesoporous zirconium phosphonate materials as efficient water-tolerable solid acid catalysts. *Catal. Sci. Technol.* **2015**, *5*, 1485–1494. [CrossRef]
67. Lin, X.Z.; Yang, Z.Z.; He, L.N.; Yuan, Z.Y. Mesoporous zirconium phosphonates as efficient catalysts for chemical CO_2 fixation. *Green Chem.* **2015**, *17*, 795–798. [CrossRef]
68. Gao, C.Y.; Ai, J.; Tian, H.R.; Wu, D.; Sun, Z.M. An ultrastable zirconium-phosphonate framework as bifunctional catalyst for highly active CO2 chemical transformation. *Chem. Commun.* **2017**, *53*, 1293–1296. [CrossRef] [PubMed]
69. Sun, L.; Kong, D.; Wang, F.; Luo, W.; Chen, Y.; Zhouzhou; Liu, J. Amorphous Porous Chromium-Zirconium Bimetallic Phosphate: Synthesis, Characterization and Application in Liquid Phase Oxidation of Hydrocarbons by Different Oxygen Sources. *ChemistrySelect* **2020**, *5*, 1552–1559. [CrossRef]
70. Zhang, P.; Kang, L.; Zhu, M.; Dai, B. Oxidative desulfurization catalyzed by a novel ZrP/MCM-41 catalyst with high performance. *Sust. Energy Fuels* **2020**, *4*, 4293–4300. [CrossRef]
71. Shashank, M.; Bhojya Naik, H.S.; Shashikanth, J.; Nizam, A.; Nagaraju, G. Green synthesis of zirconium phosphate by combustion method: Photocatalytic application and microwave-assisted catalytic conversion of aldehyde to nitriles. *Bull. Mater. Sci.* **2021**, *44*, 267. [CrossRef]
72. Ye, Z.; Chen, L.; Chen, H.; Han, L.; Chen, Q.; Wang, D. α-Zirconium phosphate nanocrystals with various morphology for photocatalysis. *Chem. Phys. Lett.* **2018**, *709*, 96–102. [CrossRef]
73. Singh, A.S.; Naikwadi, D.R.; Ravi, K.; Biradar, A.V. Chemoselective isomerization of α-Pinene oxide to trans-Carveol by robust and mild Brønsted acidic zirconium phosphate catalyst. *Mol. Catal.* **2022**, *521*, 112189. [CrossRef]
74. Machac, P.; Styskalik, A.; Moravec, Z.; Pinkas, J. Non-hydrolytic sol-gel synthesis of zirconium phosphonates with controlled mesoporosity. *Microp. Mesop. Mater.* **2023**, *362*, 112787. [CrossRef]
75. Tang, Q.; Quan, H.J.; Liu, S.; Liu, L.T.; Chow, C.F.; Gong, C.B. An environmentally friendly, photocontrollable and highly recyclable catalyst for use in a one-pot three-component Mannich reaction. *J. Mol. Catal. A Chem.* **2016**, *421*, 37–44. [CrossRef]
76. Karmakar, B.; Saha, A. A Convenient, Clean and Expeditious Synthesis of bis(heterocyclyl)methanes Over High Surface Area Zirconium Phosphate Catalyst in Water: A Green Approach. *Curr. Green Chem.* **2018**, *5*, 40–46. [CrossRef]
77. Majhi, D.; Bhoi, Y.P.; Das, K.; Pradhan, S.; Mishra, B.G. Sulfamic acid well dispersed in the micropores of Al-pillared α-ZrP as efficient heterogeneous catalyst for synthesis of structurally diverse 1,4-dihydropyridines under mild conditions. *J. Porous Mater.* **2019**, *26*, 1391–1405. [CrossRef]
78. Hajipour, A.R.; Zakery, S.; Khorsandi, Z. Synthesis of benzimidazoles by two methods (C–H functionalization and condensation reaction) catalyzed by α-zirconium hydrogen phosphate-based nanocatalyst. *J. Iran. Chem. Soc.* **2020**, *17*, 1919–1931. [CrossRef]
79. Sadraoui, K.; Ahl el haj, T.; el Mejdoubi, K.; Benzekri, Z.; el Hezzat, M.; Boukhris, S.; Sallek, B. An Efficient and Practical Process for the Synthesis of Benzimidazole and Benzothiazole Derivatives Catalyzed by Layered Zirconium Phosphate: Effect of Calcinations Temperature. *Kinet. Catal.* **2023**, *64*, 616–626. [CrossRef]

80. Ahl el haj, T.; el Mejdoubi, K.; Sadraoui, K.; El idrissi, B.C.; Sallek, B. Phosphate of Zirconium as a Reusable Efficient Catalyst for the Synthesis of 2-Arylquinazolin-4(3H)-ones. *Kinet. Catal.* **2022**, *63*, 707–715. [CrossRef]
81. John, S.E.; Gulati, S.; Shankaraiah, N. Recent advances in multi-component reactions and their mechanistic insights: A triennium review. *Org. Chem. Front.* **2021**, *8*, 4237–4287. [CrossRef]
82. Wang, J.; Wang, R.; Zi, H.; Wang, H.; Xia, Y.; Liu, X. Porous Organic Zirconium Phosphonate as Efficient Catalysts for the Catalytic Transfer Hydrogenation of Ethyl Levulinate to γ-Valerolactone without External Hydrogen. *J. Chin. Chem. Soc.* **2018**, *65*, 750–759. [CrossRef]
83. Manal, A.K.; Advani, J.H.; Srivastava, R. Bifunctional Acid-Base Zirconium Phosphonate for Catalytic Transfer Hydrogenation of Levulinic Acid and Cascade Transformation of Furfural to Biofuel Molecules. *ChemCatChem* **2022**, *14*, e202200576. [CrossRef]
84. Song, J.; Zhou, B.; Zhou, H.; Wu, L.; Meng, Q.; Liu, Z.; Han, B. Porous Zirconium–Phytic Acid Hybrid: A Highly Efficient Catalyst for Meerwein–Ponndorf–Verley Reductions. *Angew. Chem. Int. Ed.* **2015**, *54*, 9399–9403. [CrossRef]
85. Rosati, O.; Pelosi, A.; Temperini, A.; Pace, V.; Curini, M. Potassium-Exchanged Zirconium Hydrogen Phosphate [α-Zr(KPO4)2]-Catalyzed Synthesis of 2-Amino-4 H -pyran Derivatives under Solvent-Free Conditions. *Synthesis* **2016**, *48*, 1533–1540. [CrossRef]
86. Zhou, Y.; Liu, J.; Huang, R.; Zhang, M.; Xiao, M.; Meng, Y.; Sun, L. Covalently immobilized ionic liquids on single layer nanosheets for heterogeneous catalysis applications. *Dalton Trans.* **2017**, *46*, 13126–13134. [CrossRef]
87. Rosati, O.; Lanari, D.; Scavo, R.; Persia, D.; Marmottini, F.; Nocchetti, M.; Curini, M.; Piermatti, O. Zirconium potassium phosphate methyl and/or phenyl phosphonates as heterogeneous catalysts for Knoevenagel condensation under solvent free conditions. *Microp. Mesop. Mater.* **2018**, *268*, 251–259. [CrossRef]
88. Liu, B.; Ba, C.; Jin, M.; Zhang, Z. Effective conversion of carbohydrates into biofuel precursor 5-hydroxymethylfurfural (HMF) over Cr-incorporated mesoporous zirconium phosphate. *Ind. Crops Prod.* **2015**, *76*, 781–786. [CrossRef]
89. Wang, F.; Yuan, Z.; Liu, B.; Chen, S.; Zhang, Z. Catalytic oxidation of biomass derived 5-hydroxymethylfurfural (HMF) over RuIII-incorporated zirconium phosphate catalyst. *J. Ind. Eng. Chem.* **2016**, *38*, 181–185. [CrossRef]
90. Chen, M.; Xia, J.; Li, H.; Zhao, X.; Peng, Q.; Wang, J.; Gong, H.; Dai, S.; An, P.; Wang, H.; et al. A Cationic Ru(II) Complex Intercalated into Zirconium Phosphate Layers Catalyzes Selective Hydrogenation via Heterolytic Hydrogen Activation. *ChemCatChem* **2021**, *13*, 3801–3814. [CrossRef]
91. Lai, R.; Hou, Q.; Yu, G.; Xie, C.; Qian, H.; Xia, T.; Bai, X.; Tang, Y.; Rehman, M.L.U.; Ju, M. Incorporation of tin into zirconium phosphate to boost efficient conversion of trioses to lactic acid. *Catal. Commun.* **2023**, *185*, 106803. [CrossRef]
92. Xu, Y.; Lin, L.; Zeng, S.; Liu, J.; Xiao, M.; Wang, S.; Meng, Y.; Sun, L. Synthesis of Polylactide Nanocomposites Using an α-Zirconium Phosphate Nanosheet-Supported Zinc Catalyst via in Situ Polymerization. *ACS Appl. Polym. Mater.* **2019**, *1*, 1382–1389. [CrossRef]
93. Hajipour, A.R.; Karimi, H. Zinc zirconium phosphate as an efficient catalyst for chemoselective synthesis of 1,1-diacetates under solvent-free conditions. *J. Chem. Sci.* **2015**, *127*, 1945–1955. [CrossRef]
94. Karimi, H. An Efficient Selective Oxidation of Alcohols with Zinc Zirconium Phosphate under Solvent-free Conditions. *J. Chin. Chem. Soc.* **2015**, *62*, 604–613. [CrossRef]
95. Hajipour, A.R.; Karimi, H.; Kohi, A. Highly efficient and recyclable acetylation of phenols and alcohols by nickel zirconium phosphate under solvent-free conditions. *J. Iran. Chem. Soc.* **2016**, *13*, 55–64. [CrossRef]
96. Gong, H.; Zhao, X.; Qin, Y.; Xu, W.; Wei, X.; Peng, Q.; Ma, Y.; Dai, S.; An, P.; Hou, Z. Hydroformylation of olefins catalyzed by single-atom Co(II) sites in zirconium phosphate. *J. Catal.* **2022**, *408*, 245–260. [CrossRef]
97. Hajipour, A.R.; Zakery, S. α-ZrP/Uracil/Cu^{2+} nanoparticles as an efficient catalyst in the Morita-Baylis-Hillman reaction. *Appl. Organomet. Chem.* **2018**, *32*, e4487. [CrossRef]
98. Abrishami, F.; Ebrahimikia, M.; Rafiee, F. Facile synthesis of 5-substituted-1H-tetrazoles catalyzed by reusable nickel zirconium phosphate nanocatalyst. *Iran. J. Catal.* **2016**, *6*, 245–251.
99. Abrishami, F.; Daryanavard, M.; Nakhaei, F. Synthesis of 5-substituted-1H-tetrazoles using zinc zirconium phosphate and copper zirconium phosphate as reusable heterogeneous catalysts. *J. Iran. Chem. Soc.* **2023**, *20*, 1821–1829. [CrossRef]
100. Pica, M.; Nocchetti, M.; Ridolfi, B.; Donnadio, A.; Costantino, F.; Gentili, P.L.; Casciola, M. Nanosized zirconium phosphate/AgCl composite materials: A new synergy for efficient photocatalytic degradation of organic dye pollutants. *J. Mater. Chem. A* **2015**, *3*, 5525–5534. [CrossRef]
101. Kassem, M.; Harmalani, H. Effects of Structural and Textural Aspects on the Photocatalytic Performance of Zirconium Hydrogen Phosphate Doped with Tin Metal. *Kinet. Catal.* **2021**, *62*, 264–269. [CrossRef]
102. Khare, S.; Chokhare, R.; Shrivastava, P.; Kirar, J.S. Solvent-free liquid phase oxidation of styrene over iron zirconium phosphate using tert-butylhydroperoxide as an oxidant. *Indian J. Chem.* **2015**, *54*, 1032–1038.
103. He, J.; Jiang, Y.; Ding, B.; Wang, Y.; Qiu, H.; Dai, S.; Zhao, X.; Hou, Z. Zirconium phosphate supported copper catalyst for selective oxidation of phenol to cis, cis-muconic acid. *Appl. Catal. A Gen.* **2023**, *664*, 119351. [CrossRef]
104. Fu, S.; Tian, Y.; Long, X.; Shao, Q.; Wang, K.; Lei, J.; Hao, H.; Xu, Q. A new kind of hierarchical porous zirconium phosphonate: Preparation and application on oxidation catalysis. *J. Porous Mater.* **2024**. [CrossRef]
105. He, S.; Liu, X.; Zhao, H.; Zhu, Y.; Zhang, F. Zirconium phenylphosphonate-anchored methyltrioxorhenium as novel heterogeneous catalyst for epoxidation of cyclohexene. *J. Colloid Interface. Sci.* **2015**, *437*, 58–64. [CrossRef]
106. Zou, X.; Wang, C.; Wang, Y.; Shi, K.; Wang, Z.; Li, D.; Fu, X. Chiral MnIII (Salen) covalently bonded on modified ZPS-PVPA and ZPS-IPPA as efficient catalysts for enantioselective epoxidation of unfunctionalized olefins. *Polymers* **2017**, *9*, 108. [CrossRef]

107. Khare, S.; Chokhare, R.; Shrivastava, P.; Kirar, J.S.; Parashar, S. Catalytic oxidation of cyclohexene by α-zirconium phosphate intercalated Mn(Salen) using 70% tert-butylhydroperoxide as an oxidant. *Indian J. Chem.* **2016**, *55A*, 1449–1457.
108. Khare, S.; Shrivastava, P.; Chokhare, R.; Kirar, J.S.; Parashar, S. α-Zirconium phosphate supported metal–salen complex: Synthesis, characterization and catalytic activity for cyclohexane oxidation. *J. Porous Mater.* **2017**, *24*, 855–866. [CrossRef]
109. Khare, S.; Shrivastava, P. Solvent-free oxidation of cyclohexane over covalently anchored transition-metal salicylaldimine complexes to α-zirconium phosphate using tert-butylhydroperoxide. *J. Mol. Catal. A Chem.* **2016**, *411*, 279–289. [CrossRef]
110. Zhou, L.; Tu, X.B.; Yang, Z.Y.; Wei, D.J.; Lu, W. Efficient and recyclable performance of organic-inorganic zirconium phosphonates supported salen-Mn(III) as catalysts for CO_2 cycloaddition. *IOP Conf. Ser. Mater. Sci. Eng.* **2019**, *479*, 012020. [CrossRef]
111. Zhou, L.; Gong, B.; Yang, Z.; Wei, D.; Lu, W. Application of Modified Organic-Inorganic Hybrid Zirconium Phosphate Material ZAMPS-PVPA-Salen-Mn(III) in Chemical Fixation of CO_2. *IOP Conf. Ser. Mater. Sci. Eng.* **2019**, *472*, 012076. [CrossRef]
112. Liao, H.; Jiang, Y.; Wei, X.; Zhao, X.; Lai, W.; An, N.; Ma, Y.; Dai, S.; Hou, Z. Intercalated Zirconium Phosphate Promotes Reductive Amination of Carbon Dioxide. *ACS Sust. Chem. Eng.* **2024**, *12*, 2632–2645. [CrossRef]
113. Kanchi, S.; Ahmed, S. (Eds.) *Green Metal Nanoparticles: Synthesis, Characterization and Their Applications*; Wiley-Scrivener: Hoboken, NJ, USA, 2018. [CrossRef]
114. El Shafey, A.M. Green synthesis of metal and metal oxide nanoparticles from plant leaf extracts and their applications: A review. *Green Process. Synth.* **2020**, *9*, 304–339. [CrossRef]
115. Kumar, A.; Choudhary, P.; Kumar, A.; Camargo, P.H.; Krishnan, V. Recent advances in plasmonic photocatalysis based on TiO2 and noble metal nanoparticles for energy conversion, environmental remediation, and organic synthesis. *Small* **2022**, *18*, 2101638. [CrossRef]
116. Nocchetti, M.; Donnadio, A.; Vischini, E.; Posati, T.; Albonetti, C.; Campoccia, D.; Arciola, C.R.; Ravaioli, S.; Mariani, V.; Montanaro, L.; et al. Synthesis, Crystal Structure, and Antibacterial Properties of Silver-Functionalized Low-Dimensional Layered Zirconium Phosphonates. *Inorg. Chem.* **2022**, *61*, 2251–2264. [CrossRef]
117. Piermatti, O. Green Synthesis of Pd Nanoparticles for Sustainable and Environmentally Benign Processes. *Catalysts* **2021**, *11*, 1258. [CrossRef]
118. Valentini, V.; Piermatti, O.; Vaccaro, L. Metal and Metal Oxide Nanoparticles Catalyzed C–H Activation for C–O and C–X (X = Halogen, B, P, S, Se) Bond Formation. *Catalysts* **2023**, *13*, 16. [CrossRef]
119. Sápi, A.; Rajkumar, T.; Kiss, J.; Kukovecz, Á.; Kónya, Z.; Somorjai, G.A. Metallic nanoparticles in heterogeneous catalysis. *Catal. Lett.* **2021**, *151*, 2153–2175. [CrossRef]
120. Ohtaka, A. Recent Progress of Metal Nanoparticle Catalysts for C–C Bond Forming Reactions. *Catalysts* **2021**, *11*, 1266. [CrossRef]
121. Ndolomingo, M.J.; Bingwa, N.; Meijboom, R. Review of supported metal nanoparticles: Synthesis methodologies, advantages and application as catalysts. *J. Mater. Sci.* **2020**, *55*, 6195–6241. [CrossRef]
122. Kobayashi, S. (Ed.) *Nanoparticles in Catalysis*; Springer: Berlin/Heidelberg, Germany, 2020. [CrossRef]
123. Hu, H.; Xin, J.H.; Hu, H.; Wang, X.; Miao, D.; Liu, Y. Synthesis and stabilization of metal nanocatalysts for reduction reactions–a review. *J. Mater. Chem. A* **2015**, *3*, 11157–11182. [CrossRef]
124. Tao, F.F. *Metal Nanoparticles for Catalysis: Advances and Applications*, 1st ed.; Royal Society of Chemistry: Cambridge, UK, 2014.
125. Zhu, C.; Liu, Q.; Li, D.; Wang, H.; Zhang, C.; Cui, C.; Chen, L.; Cai, C.; Ma, L. Selective Hydrodeoxygenation of 5-Hydroxymethylfurfural to 2,5-Dimethylfuran over Ni Supported on Zirconium Phosphate Catalysts. *ACS Omega* **2018**, *3*, 7407–7417. [CrossRef]
126. Ma, H.; Li, H.; Zhao, W.; Li, L.; Liu, S.; Long, J.; Li, X. Selective depolymerization of lignin catalyzed by nickel supported on zirconium phosphate. *Green Chem.* **2019**, *21*, 658–668. [CrossRef]
127. Choudhary, H.; Das, L.; Pelton, J.G.; Sheps, L.; Simmons, B.A.; Gladden, J.M.; Singh, S. Funneled Depolymerization of Ionic Liquid-Based Biorefinery "Heterogeneous" Lignin into Guaiacols over Reusable Palladium Catalyst. *Chem. Europ. J.* **2023**, *29*, 330. [CrossRef]
128. Gong, H.; Zhou, C.; Cui, Y.; Dai, S.; Zhao, X.; Luo, R.; An, P.; Li, H.; Wang, H.; Hou, Z. Direct Transformation of Glycerol to Propanal using Zirconium Phosphate-Supported Bimetallic Catalysts. *ChemSusChem* **2020**, *13*, 4954–4966. [CrossRef]
129. Luo, R.; Zhao, X.; Gong, H.; Qian, W.; Li, D.; Chen, M.; Cui, K.; Wang, J.; Hou, Z. Effect of Tungsten Modification on Zirconium Phosphate-Supported Pt Catalyst for Selective Hydrogenolysis of Glycerol to 1-Propanol. *Energy Fuels* **2020**, *34*, 8707–8717. [CrossRef]
130. Ye, Y.; Wang, H.; Zhang, Y.; Zhao, H.; Du, W.; Chen, P.; Hou, Z. Catalytic recycling of polylactic acid over zirconium phosphate supported WOx active sites. *Appl. Catal. A Gen.* **2024**, *686*, 119917. [CrossRef]
131. Liu, X.; Liu, X.; Li, N.; Ma, P.; Zhang, Y. Direct synthesis of hexitols from microcrystalline cellulose and birch over zirconium(iv) phosphate supported nickel catalysts and the mechanism study. *Green Chem.* **2021**, *23*, 1353–1360. [CrossRef]
132. Han, G.H.; Lee, M.W.; Park, S.; Kim, H.J.; Ahn, J.P.; Seo, M.-G.; Lee, K.Y. Revealing the factors determining the selectivity of guaiacol HDO reaction pathways using ZrP-supported Co and Ni catalysts. *J. Catal.* **2019**, *377*, 343–357. [CrossRef]
133. Gao, J.; Cao, Y.; Luo, G.; Fan, J.; Clark, J.H.; Zhang, S. High-efficiency catalytic hydrodeoxygenation of lignin-derived vanillin with nickel-supported metal phosphate catalysts. *Chem. Eng. J.* **2022**, *448*, 137723. [CrossRef]
134. Li, D.; Gong, H.; Lin, L.; Ma, W.; Zhou, Q.; Kong, K.; Huang, R.; Hou, Z. Selective aerobic oxidation of glycerol over zirconium phosphate-supported vanadium catalyst. *Mol. Catal.* **2019**, *474*, 110404. [CrossRef]

135. Li, X.; Ding, G.; Thompson, B.L.; Hao, L.; Deming, D.A.; Heiden, Z.M.; Zhang, Q. Microwave-Assisted Synthesis of Zirconium Phosphate Nanoplatelet-Supported Ru-Anadem Nanostructures and Their Catalytic Study for the Hydrogenation of Acetophenone. *ACS Appl. Mater. Interfaces* **2020**, *12*, 30670–30679. [CrossRef]
136. Borah, G.; Borborah, A.; Gogoi, N. α-ZrP-supported CdS quantum dot composite material: An efficient and recyclable photocatalyst for selective oxidation of benzyl alcohol. *Bull. Mater. Sci.* **2022**, *45*, 136. [CrossRef]
137. Zhou, Y.; Wang, A.; Wang, Z.; Chen, M.; Wang, W.; Sun, L.; Liu, X. Titanium functionalized α-zirconium phosphate single layer nanosheets for photocatalyst applications. *RSC Adv.* **2015**, *5*, 93969–93978. [CrossRef]
138. Costantino, F.; Vivani, R.; Bastianini, M.; Ortolani, L.; Piermatti, O.; Nocchetti, M.; Vaccaro, L. Accessing stable zirconium carboxy-aminophosphonate nanosheets as support for highly active Pd nanoparticles. *Chem. Commun.* **2015**, *51*, 15990–15993. [CrossRef]
139. Kozell, V.; Giannoni, T.; Nocchetti, M.; Vivani, R.; Piermatti, O.; Vaccaro, L. Immobilized palladium nanoparticles on zirconium carboxy-aminophosphonates nanosheets as an efficient recoverable heterogeneous catalyst for Suzuki–Miyaura and Heck coupling. *Catalysts* **2017**, *7*, 186. [CrossRef]
140. Borah, S.; Mishra, S.; Cardenas, L.; Gogoi, N. Pd Nanoparticles Dispersed on ZrIV Organophosphonate: A Robust and Reusable Catalyst for Suzuki–Miyaura Cross-Coupling Reactions. *Eur. J. Inorg. Chem.* **2018**, *2018*, 751–758. [CrossRef]
141. Bhattacharyya, B.; Biswas, J.P.; Mishra, S.; Gogoi, N. Rapid Suzuki-Miyaura cross-coupling reaction catalyzed by zirconium carboxyphosphonate supported mixed valent Pd(0)/Pd(II) catalyst. *Appl. Organomet. Chem.* **2019**, *33*, 5017. [CrossRef]
142. Petrucci, C.; Cappelletti, M.; Piermatti, O.; Nocchetti, M.; Pica, M.; Pizzo, F.; Vaccaro, L. Immobilized palladium nanoparticles on potassium zirconium phosphate as an efficient recoverable heterogeneous catalyst for a clean Heck reaction in flow. *J. Mol. Catal. A Chem.* **2015**, *401*, 27–34. [CrossRef]
143. Zhou, J.; Sun, H.; Xu, C.; Wang, Z.; Zhang, H.; Guo, D.; Zhang, J.; Ji, X.; Liu, L.; Ma, J.; et al. Palladium nanoparticles supported on α-zirconium phosphate nanosheets as a highly efficient heterogeneous catalyst for the Heck reaction. *J. Taiwan Inst. Chem. Eng.* **2022**, *138*, 104478. [CrossRef]
144. Costantino, F.; Nocchetti, M.; Bastianini, M.; Lavacchi, A.; Caporali, M.; Liguori, F. Robust Zirconium Phosphate-Phosphonate Nanosheets Containing Palladium Nanoparticles as Efficient Catalyst for Alkynes and Nitroarenes Hydrogenation Reactions. *ACS Appl. Nano Mat.* **2018**, *1*, 1750–1757. [CrossRef]
145. Ferlin, F.; Cappelletti, M.; Vivani, R.; Pica, M.; Piermatti, O.; Vaccaro, L. Au@zirconium-phosphonate nanoparticles as an effective catalytic system for the chemoselective and switchable reduction of nitroarenes. *Green Chem.* **2019**, *21*, 614–626. [CrossRef]
146. Zhou, Y.; Ding, H.; Liu, J.; LaChance, A.M.; Xiao, M.; Meng, Y.; Sun, L. Gold nanoparticles immobilized on single-layer α-zirconium phosphate nanosheets as a highly effective heterogeneous catalyst. *Adv. Compos. Hybrid Mater.* **2019**, *2*, 520–529. [CrossRef]
147. Lai, G.H.; Huang, T.C.; Pai, Y.H.; Huang, B.S.; Tsai, M.H.; Yang, T.I.; Chung, Y.H. Preparation of highly-stable and recyclable novel Au/ZrP composite catalyst for 4-nitrophenol reduction. *J. Taiwan Inst. Chem. Eng.* **2019**, *95*, 525–531. [CrossRef]
148. Gong, H.; Lin, L.; Zhao, X.; Li, H.; Li, D.; Xu, Z.; Chen, M.; Huang, R.; Hou, Z. Atomically precise Ag nanoclusters intercalated in zirconium pyrophosphate for efficient hydrogenation of nitroaromatics. *Appl. Catal. A Gen.* **2019**, *574*, 1–9. [CrossRef]
149. Xu, Y.; Zhou, F.; Chen, M.; Hu, H.; Lin, L.; Wu, J.; Zhang, M. Facile assembly of 2D α-zirconium phosphate supported silver nanoparticles: Superior and recyclable catalysis. *New J. Chem.* **2020**, *44*, 9793–9801. [CrossRef]
150. Lin, L.; Wen, Y.; Li, L.; Tan, Y.; Yang, P.; Liang, Y.; Xu, Y.; Hu, H.; Xu, Y. Mussel-Inspired Surface Modification of α-Zirconium Phosphate Nanosheets for Anchoring Efficient and Reusable Ultrasmall Au Nanocatalysts. *Nanomaterials* **2022**, *12*, 3339. [CrossRef] [PubMed]
151. Qin, Y.; Jiang, Y.; Wei, X.; Ma, Y.; Liao, H.; Peng, Q.; Dai, S.; Wang, Z.; Zhao, X.; Hou, Z. Zirconium phosphate supported-silver nanoparticles for selective hydrogenation of nitrobenzene into azoxybenzene compounds. *New J. Chem.* **2023**, *47*, 14380–14394. [CrossRef]
152. Zhang, F.; Jiang, Y.; Dai, S.; Wei, X.; Ma, Y.; Liao, H.; Qin, Y.; Peng, Q.; Zhao, X.; Hou, Z. Selective Hydrogenation of Nitrobenzene to para-Aminophenol on a Zirconium-Phosphate-Supported Platinum Catalyst. *Ind. Eng. Chem. Res.* **2023**, *62*, 5814–5825. [CrossRef]
153. Awaya, K.; Sato, Y.; Miyazaki, A.; Furukubo, M.; Nishiyama, K.; Tsushida, M.; Ida, S.; Ohyama, J.; Machida, M. Selective catalytic NOx reduction by H_2 in excess O_2 over Pt/zirconium phosphate nanosheets. *Catal. Sci. Technol.* **2024**, *14*, 6055–6064. [CrossRef]
154. Lawrence, S.A. *Amines: Synthesis, Properties and Applications*; Cambridge University Press: Cambridge, UK, 2004.
155. Rosenblatt, D.H.; Burrows, E.P. *The Chemistry of Amino, Nitroso, and Nitro Compounds and Their Derivatives*; Patai, S., Ed.; John Wiley &Sons: Chichester, UK, 1982; p. 1085.
156. Nishimura, S. *Handbook of Heterogeneous Catalytic Hydrogenation for Organic Synthesis*; John Wiley & Sons: New York, NY, USA, 2001; pp. 315–387.
157. Mitchell, S.C.; Waring, R.H. *Ullmanns Encyclopedia of Industrial Chemistry*; Wiley-VCH: Weinheim, Germany, 2000.
158. Hu, Z.N.; Liang, J.; Ding, K.; Ai, Y.; Liang, Q.; Sun, H.B. Insight into the selectivity of nano-catalytic nitroarenes reduction over other active groups by exploring hydrogen sources and metal components. *Appl. Catal. A Gen.* **2021**, *626*, 118339. [CrossRef]
159. Blaser, H.U.; Steiner, H.; Studer, M. Selective catalytic hydrogenation of functionalized nitroarenes: An update. *ChemCatChem* **2009**, *1*, 210–221. [CrossRef]
160. Kadam, H.K.; Tilve, S.G. Advancement in methodologies for reduction of nitroarenes. *RSC Adv.* **2015**, *5*, 83391–83407. [CrossRef]

161. Begum, R.; Rehan, R.; Farooqi, Z.H.; Butt, Z.; Ashraf, S. Physical chemistry of catalytic reduction of nitroarenes using various nanocatalytic systems: Past, present, and future. *J. Nanopart. Res.* **2016**, *18*, 231. [CrossRef]
162. Sedghi, R.; M Heravi, M.; Asadi, S.; Nazari, N.; R Nabid, M. Recently used nanocatalysts in reduction of nitroarenes. *Curr. Org. Chem.* **2016**, *20*, 696–734. [CrossRef]

Disclaimer/Publisher's Note: The statements, opinions and data contained in all publications are solely those of the individual author(s) and contributor(s) and not of MDPI and/or the editor(s). MDPI and/or the editor(s) disclaim responsibility for any injury to people or property resulting from any ideas, methods, instructions or products referred to in the content.